NASA CONTRACTOR REPORT

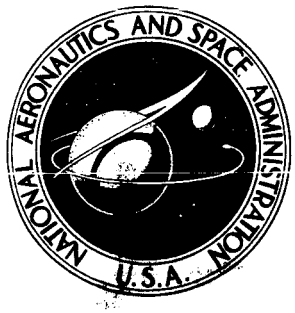

NASA CR-2414

NASA CR-2414

SEPARATED FLOW OVER BODIES OF REVOLUTION USING AN UNSTEADY DISCRETE-VORTICITY CROSS WAKE

Part I - Theory and Application

by F. J. Marshall and F. D. Deffenbaugh

Prepared by
PURDUE UNIVERSITY
West Lafayette, Ind.
for Langley Research Center

NATIONAL AERONAUTICS AND SPACE ADMINISTRATION • WASHINGTON, D. C. • JUNE 1974

1. Report No.	2. Government Accession No.	3. Recipient's Catalog No.
NASA CR-2414		

4. Title and Subtitle	5. Report Date
SEPARATED FLOW OVER BODIES OF REVOLUTION USING AN UNSTEADY DISCRETE-VORTICITY CROSS WAKE - PART I THEORY AND APPLICATION	June 1974
	6. Performing Organization Code
7. Author(s)	8. Performing Organization Report No.
F.J. Marshall and F.D. Deffenbaugh	
9. Performing Organization Name and Address	10. Work Unit No.
Purdue University School of Aeronautics and Astronautics W. Lafayette, Indiana	760-65-11-0200
	11. Contract or Grant No.
	NGR 15-005-119 (181)
12. Sponsoring Agency Name and Address	13. Type of Report and Period Covered
National Aeronautics and Space Administration Washington, DC 20546	Contractor Report
	14. Sponsoring Agency Code

15. Supplementary Notes

Topical report.

16. Abstract

A method is developed to determine the flow field of a body of revolution in separated flow. The technique employed is the use of the computer to integrate various solutions and solution properties of the sub-flow fields which made up the entire flow field without resorting to a finite difference solution to the complete Navier-Stokes equations. The technique entails the use of the unsteady cross flow analogy and a new solution to the required two-dimensional unsteady separated flow problem based upon an unsteady, discrete-vorticity wake. Data for the forces and moments on aerodynamic bodies at low speeds and high angle of attack (outside the range of linear inviscid theories) such that the flow is substantially separated are produced which compare well with experimental data. In addition, three dimensional steady separation regions and wake vortex patterns are determined.

17. Key Words (Suggested by Author(s))	18. Distribution Statement
Bodies of Revolution Unsteady flow Separated Flow Crossflow Flow field	Unclassified STAR Category 12

19. Security Classif. (of this report)	20. Security Classif. (of this page)	21. No. of Pages	22. Price*
Unclassified	Unclassified	91	$4.00

*For sale by the National Technical Information Service, Springfield, Virginia 22151

TABLE OF CONTENTS

SUMMARY

A method has been developed to determine the flow field of a body of revolution in steady separated flow (e.g. at high angle of attack), including the prediction of the normal force and pitching moment.

The method makes use of a computer to integrate the various solutions and solution properties of the sub-flow fields which make up the entire flow field. Thus, a finite difference solution to the complete Navier-Stokes equations is not employed.

The method utilizes two ideas in this approach to a steady three-dimensional separated flow: the unsteady cross flow analogy which reduces the given three-dimensional steady separated flow to a two-dimensional unsteady separated flow and a new solution technique for the latter problem. This technique employs a wake description of discrete point vortices arising from the separation of shear layers at the surface. The point vortices convect and diffuse downstream to form an unsteady wake. Thus the mathematical model follows directly from the physics of the wake evolution with time.

The overall technique is applied, employing a computer, to two test cases: an ogive-cylinder and an ellipsoid of revolution at low speeds. Force and moment data are obtained and are found to agree well with experimental data, particularly at high angles of attack where inviscid theory is invalid. Separation regions and wake patterns are found which agree with available experimental findings.

1.0 Introduction

The objective of the present work is to develop a numerical computation method to determine the flow field of a body of revolution in steady separated flow (e.g., a body at high angle of attack), including the prediction of forces and moments.

There are many computational techniques of varying accuracy for the flow about a body with no separation such that the assumptions of inviscid flow and linearized equations of motion can be utilized (references 1 & 2, for example). For such flow fields the techniques are based upon the availability of fundamental solutions of the equations of motion in integral form but with unknown singularity distributions. The computer is then used to determine specific solutions for the particular bodies which meet imposed boundary conditions and to evaluate the resulting numerical solution to yield pressure distributions, forces and moments. For flow fields in which separation must be taken into account, the assumptions of inviscid flow and linearized theory are invalid and the usual approach is to solve the Navier-Stokes equations in finite-difference form by means of a computer (references 3, 4, 5). At present, the solutions for inviscid, linear flow are more developed and hence, more reliable, and require far less computation than the full finite difference solutions.

It is intended here to adopt the former approach; i.e., computer implementation of known solutions and solution properties. This approach is believed to promote an increased physical understanding

of the problem, to reduce the role of the computer as a black box, and to minimize the computational time and storage.

The obstacle in pursuing such a course is, obviously, the relatively very few solutions and solution properties for viscous flows compared to the situation for inviscid flows. To overcome this obstacle, two techniques are employed.

The first is the unsteady cross flow analogy (or viscous cross flow analogy or impulse flow analogy), which is based upon the assumption of an equivalence between three dimensional steady flow and two dimensional unsteady flow. As explained in more detail below, this assumption is a heuristic one based primarily upon experimental data. With this technique, the three dimensional steady separated flow problem is reduced to a two dimensional unsteady separated flow problem.

The second technique, applicable to the latter problem, is based upon the assumption that the two dimensional unsteady wake can be described by a distribution of inviscid point vortices superimposed on the unseparated potential flow solution, suitably modified by diffusive effects. The argument for this is based upon the time evolution of the wake.

Part I of the report treats the basic theory, applications and results while Part II describes the computer program.

In the following sections of this part, Part I, the basic theory consists of the description of the unsteady cross flow analogy and the solution technique for the flow in the cross plane, a two dimensional

unsteady flow field. The theory is applied to two geometries, an ogive-cylinder and an ellipsoid of revolution and results for normal force, pitching moment, vortex-wake patterns and separation regions are compared with experimental data.

List of Symbols

$a(t)$	radius as function of time (Figure 2)
$\tilde{a}$	characteristic length of two dimensional unsteady flow field
d	maximum body diameter (Figure 1)
f	fineness ration (= ℓ/d)
$C_{D,p}$	coefficient of drag due to pressure (equation (22))
C_D	coefficient of drag (equation (13))
$C_{M,\lambda}$	coefficient of pitching moment about point $[0,0,\lambda\hat{z}]$
c_n	coefficient of sectional normal force (equation (6))
C_N	coefficient of normal force (equation (7))
$c_{n,p}$	coefficient of sectional normal force due to pressure (equation (19))
C_p	coefficient of [illegible]ations (12) and (18))
D	drag (equation (11))
$H(t)$	step function (= 0, $t \leq 0$, = 1, $t \leq 0$)
ℓ	body length (Figure 1)
$\ell_{\beta k}$	distance of vortex from origin (= $[x_{\beta k}^2 + y_{\beta k}^2]^{1/2}$)
m_k	location of vortex born from boundary layer (equation (44))
m_{rk}	location of vortex born from rear shear layer (equation (47))
M	pitching moment (equation (4))
N	normal force (equation (31))
p	pressure
q	dynamic pressure
r	polar radius (Figure 3)
r_o	body radius (Figure 1)
r_c	vortex core radius (Figure 7)

$\bar{r}$	boundary layer variable (equation (37))
Re_{3DS}	Reynolds number, three dimensional steady ($= V\ell/\nu$)
Re_{2DUS}	Reynolds number, two dimensional unsteady ($= U\tilde{a}/\nu$)
t	time
S	frontal area
S_B	base area
U	$= V \sin \alpha$ (Figure 1)
V	free stream velocity (Figure 1)
W	$= V \cos \alpha$ (Figure 1)
$[\tilde{u},\tilde{v}]$	cartesian velocity components (Figure 3)
[u,v]	polar velocity components (Figure 3)
[x,y,z,t]	coordinates (Figure 2)

Greek

α	angle of attack (Figure 1)
Γ	circulation
δ	$= 1/\sqrt{Re_{2DUS}}$
θ	polar angle (Figure 3)
λ	moment arm coefficient ($0 \leq \lambda \leq 1$)
ν	kinematic viscosity
ρ	density
σ	vortex flux coefficient ($0 < \sigma \leq 1$)
τ	wall shear stress
Φ	potential function
Ψ	stream function
ω	vorticity

Sub- and Superscript

$( )^*$	dimensional
$( )^\circ$	outer flow
$( )_\circ^\circ$	outer flow evaluated at surface
$( )^i$	inner flow
$(\bar{\ })$	inner flow
$( )^f$	forward
$( )^r$	rear
$( )_m$	extremum
$( )_\circ$	stagnation point
$( )_s$	separation point
$( )_k$	at time t_k
$( )_{\beta k}$	point vortex β at time t_k
$( )_\infty$	freestream value
$( )_{,r}$, $( )_{,\theta}$, $( )_{,t}$	partial derivatives

Miscellaneous

$(\hat{\ })$		three dimensional steady flow (in contradistinction to $( )$, two dimensional unsteady flow)
$(\dot{\ })$	$\equiv$	$\frac{d( )}{dt}$
$\Delta\theta$, $\Delta\bar{r}$, $\Delta t_k = t_{k+1} - t_k$		numerical integration parameters

2.0 Unsteady Cross Flow

2.1 General Concepts

The problem is to determine the flow field and to predict the forces and moments on a three-dimensional body of angle of attack α in a steady uniform flow (Figure 1) at high Reynolds number. The angle of attack α is of arbitrary magnitude such that the flow may be separated. Thus linearized theory is not sufficient.

For aerodynamic bodies at small angles of attack, the three dimensional boundary layer adheres to the entire body except in the neighborhood of a small base. For this situation the boundary layer may be ignored allowing for an inviscid flow approximation and, for slender bodies, application of linearized theory. For higher angles of attack (references 6-10) the boundary layer separates and may separate to such an extent that flow separation exists over a substantial portion of the body surface. In this situation, inviscid theory is no longer applicable (even though the body is slender) and there is no viscous theory to describe this complicated three dimensional flow field.

This problem is approached herein by using the unsteady cross flow analogy applied to a body of revolution (references 11-23). The essence of this technique is found in applying the (dimensional) transformation $[\hat{x}^*, \hat{y}^*, \hat{z}^*, \hat{t}^*] = [x^*, y^*, z^* + Wt^*, t^*]$ and considering the flow field in the plane $z^* = 0$ (see Figure 1). In this plane, the flow field is that induced by a circular cylinder of time-varying radius (correlated with the thickness distribution of the body) in a

uniform, viscous, incompressible free stream of velocity $U = V \sin \alpha$.

Information available from the relatively simpler two-dimensional unsteady flow is thus applicable to the three-dimensional steady flow field. In particular, the two-dimensional unsteady drag distribution with time is applicable. This can be transformed to the longitudinal normal force distribution of the three dimensional steady flow field yielding the normal force and pitching moment on the given body at angle of attack.

The correlation of the two dimensional unsteady results and the three dimensional steady results lacks a theoretical foundation (references 13, p. 415 and 24, p. 464). Basically, there exists no general transformation between the two dimensional unsteady and the three dimensional steady Navier-Stokes equations. There exist particular transformations such as in slender body theory and its extension to hypersonic flow, the equivalence principle, and it is of note that these are inviscid theories (shocks entering by jump conditions). So, to this date, the prime argument for the validity of the unsteady cross flow analogy lies in the similarity of the flow fields obtained, usually by vortex visualization techniques, and the valid results achieved, although the latter can be argued against on the grounds of empiricism.

The question of the existence of a transformation between three dimensional steady and two dimensional unsteady Navier-Stokes equations can be considered in terms of a basic property of the unsteady cross flow analogy, namely, the absence of upstream effects; the force

distribution on the three dimensional body over the length $(0, \hat{z}^*)$ is independent of the force distribution over the length $(\hat{z}^*, \ell)$. For this to be true the steady Navier-Stokes equations would have to be parabolic or hyperbolic with $\hat{z}^*$ as a time-like coordinate.

If the three dimensional steady flow field is decomposed into the outer inviscid flow, the boundary layer, and the wake, the governing equation would be the Euler equations, the boundary layer equations, and the complete Navier-Stokes equations, respectively.

For incompressible flow (reference 25), the outer flow is governed by elliptic equations, the boundary layer by parabolic equations with $\hat{z}$ time-like, and the wake by elliptic equations. Thus only the boundary layer region is compatible with the unsteady cross flow property.

For supersonic flow the theory is not as well developed. The outer flow is governed by elliptic equations (which mathematically may be ignored for a sharp pointed body) and hyperbolic equations. The boundary layer is still parabolic but the complete Navier-Stokes equations in the wake still have an elliptic property.

Thus, aside from shocks, the requirements for the validity of the unsteady cross flow analogy are partially met in supersonic flow in that the outer flow is for the most part hyperbolic but in the dominant region, the wake, the requirements are not satisfied.

While the boundary layer of the three dimensional steady flow field is parabolic, there is the conflict between three dimensional and two dimensional boundary layer states (reference 13, p. 415). For usual three dimensional flow fields, the three dimensional boundary

layer is for the most part turbulent. Yet the pertinent Reynolds' number for two-dimensional unsteady flow, a function of the Reynolds' number of the three dimensional steady flow, could be such that a two dimensional laminar boundary layer theoretically exists. This mathematical result has no physical interpretation. For the particular three dimensional steady flow fields considered herein and for the particular equivalence between three dimensional steady and two-dimensional unsteady flow fields used herein, the pertinent Reynolds' number determined for the latter flow field are such that laminar boundary layers theoretically exist. Thus the use of laminar two dimensional unsteady boundary layers are employed based upon this formal justification.

In addition there is the discrepancy between the concept of two dimensional and three dimensional separation of boundary layers, further complicated by the unsteadiness of the two dimensional boundary layer.

There exists a body of work employing the application of the unsteady cross flow analogy to a delta wing of low aspect ratio. This problem has the advantage in that the sub-problem of the two dimensional unsteady flow (about a flat plate or thin ellipse as opposed to a circular cylinder) is simpler since the location of the separation point is known a priori (i.e. the flow separates almost immediately at the edge). In addition, the delta wing can be approached by assuming a conical flow in the three dimensional steady case which bears resemblance to the two dimensional unsteady case (reference 26). This area has received a great deal of attention (references 27-30) but the present work cannot make use of these simplifications.

The work of Hill for bodies of revolution (reference 31), while not employing the explicit cross flow analogy, bears upon the problem of separated flow. The theory is completely inviscid and so the approach is a limited one.

In this context then it is not surprising that the correlation between the two flow fields has been achieved in various ways, often requiring ad hoc experimental data. The correlation used in this work (see Section 2.2) is the direct one of equating two dimensional unsteady drag (pressure and viscous, although the latter is usually negligible) to the normal force distribution.

The sub-problem of two-dimensional unsteady flow while simpler to treat than the original three dimensional steady one, is still a difficult problem since a boundary layer forms, separates, and a wake is formed about a cylinder of varying radius. This sub-problem,discussed more fully in Section 3.0, is treated with a new approach compatible with the originally defined approach of using the computer with known solutions. With the possible exception of reference 17, (which uses a finite difference approximation to the Navier-Stokes equation) this approach yields the most complete model (for high Reynolds' number) in that viscosity enters directly and empiricism is minimized.

2.2 Transformations

In the absence of a transformation between the three dimensional steady and two dimensional unsteady Navier-Stokes equations, the unsteady cross flow analogy is applied by utilizing simple transformations of the geometries and the forces.

The geometry transformations obtained as follows: given the three dimensional steady flow field of Figure 1. If a velocity $W = V \cos \alpha$ is superimposed on the steady three dimensional flow field of Figure 1, the flow field of Figure 2a results. Then if attention is confined to the plane $\hat{z}^* = 0$, the situation is that of an unsteady two dimensional flow field with a constant velocity at infinity and body radius changing with time, Figure 2b.

The geometry transformations are then, with $(\,)^*$ as a dimensional quantity,

$$a^*(t^*) = r_o^*(\hat{z}^*), \quad t^* = \frac{\hat{z}^*}{W}; \quad 0 \le \hat{z}^* \le \ell, \; 0 \le t^* \le \frac{\ell}{W} \tag{1}$$

for arbitrary $r_o^*(\hat{z}^*)$.

Now r_o^* is normalized by $d/2$. In the unsteady two dimensional problem, $a^*(t^*)$ must be normalized by a length characteristic of the problem. Let this characteristic length be $\tilde{a}$ to be defined for each particular body but on the order of $(W/\ell) \int_0^{W/\ell} a^*(t^*)dt^* = (1/\ell) \cdot \int_0^{\ell} r_o^*(\hat{z}^*)d\hat{z}^*$.

Letting $t = Ut^*/\tilde{a}$, the above equations in nondimensional form are

$$a(t) = \left(\frac{d}{2\tilde{a}}\right) r_o(\hat{z}), \quad t = \left(\frac{df}{\tilde{a}} \tan \alpha\right) \hat{z}; \quad 0 \le \hat{z} \le 1, \; 0 \le t \le \frac{df \tan \alpha}{\tilde{a}} \tag{2}$$

The force transformation is obtained as follows: given the three dimensional steady flow field of Figure 1. The normal, force, N, and the pitching moment, M, are to be determined utilizing the unsteady cross flow analogy.

Consider the three dimensional steady flow field. Let $N(\hat{z}^*)$ be the force normal to axis of symmetry on the section of the body from the nose to $\hat{z}^*$ such that $N(\ell) \equiv N$. Then

$$N = \int_o^{\ell} \frac{dN}{d\hat{z}^*} d\hat{z}^* \tag{3}$$

The moment about the nose is then, positive nose up,

$$M = -\int_o^{\ell} [\hat{z}^* + r_o^* \frac{dr_o}{d\hat{z}^*}] \frac{dN}{d\hat{z}^*} d\hat{z}^* \tag{4}$$

and the moment about an arbitrary point $[\hat{x},\hat{y},\hat{z}] = [0,0,\lambda\ell]$, $0 \leq \lambda \leq 1$, is

$$M_\lambda = M + \lambda\ell N \tag{5}$$

To reduce these to coefficient form let

$$c_n(\hat{z}) = \frac{2 \frac{dN}{d\hat{z}^*}}{\hat{\rho}V^2 d} \tag{6}$$

$$C_N = \frac{2N}{\hat{\rho}V^2 S} \tag{7}$$

$$C_{M,\lambda} = \frac{2M_\lambda}{\hat{\rho}V^2 S\ell} \tag{8}$$

where d is the maximum diameter, ℓ is the length and $S = \pi d^2/4$ the frontal area.

Normalizing $\hat{z}^*$ by ℓ, equations (3), (4) and (5) become

$$C_N = \frac{4f}{\pi} \int_o^1 c_n \, d\hat{z} \tag{9}$$

$$C_{M,\lambda} = -\frac{4f}{\pi} \int_o^1 [\hat{z} + \frac{r_o}{4f^2} \frac{dr_o}{d\hat{z}}] \, c_n \, d\hat{z} + \lambda C_N \tag{10}$$

The above coefficients are found by solving the two dimensional unsteady problem. Within this problem, the pertinent force is the drag as a function of time. (It is assumed that the times are not long enough for any oscillating lift to develop).

The drag is given by

$$D(t^*) = \int_o^{2\pi} p^* \cos\theta \; a^*(t^*) d\theta + \int_o^{2\pi} \tau^* \sin\theta \; a^*(t^*) d\theta \qquad (11)$$

With a coefficient of pressure

$$C_p = \frac{2(p^* - p^*_\infty)}{\rho U^2} \qquad (12)$$

the coefficient of drag

$$C_D = \frac{2D}{\rho U^2 (2\tilde{a})} \qquad (13)$$

is obtained as

$$C_D(t) = \frac{1}{2} \int_o^{2\pi} C_p \cos\theta \; a(t) d\theta + \frac{1}{2} \int_o^{2\pi} \tau \sin\theta \; a(t) d\theta \qquad (14)$$

where $\tau = 2\tau^*/\rho U^2$.

Then the basic assumption in the force transformation is

$$\frac{dN}{d\hat{z}^*}(\hat{z}^*) = D(t^*), \quad \hat{z}^* = Wt^*; \quad \hat{\nu} = \nu, \; \hat{\rho} = \rho, \; \hat{p}_\infty = p_\infty \qquad (15)$$

or in non-dimensional form

$$c_n(\hat{z}) = \frac{2\tilde{a}}{d} \sin^2\alpha \; C_D(t); \quad \hat{z} = \frac{\tilde{a}t}{df \tan\alpha} \qquad (16)$$

with $Re_{2DUS} = Re_{3DS} \; (\tilde{a}/fd) \sin\alpha$ and the same free stream static values.

This assumption ignores longitudinal shear effects. But for aerodynamics shapes the fineness ratio f = ℓ/d is usually large, thus reducing the contribution of longitudinal effects.

To further check the assumptions, comparisons were made between the experimental pressure distributions of the three dimensional steady flow and the theoretically derived two dimensional unsteady ones. To make this comparison let $N_p(\hat{z}^*)$ be the normal force due to pressure only on the segment of the body from the nose to $\hat{z}^*$ in the three dimensional steady flow. Then

$$\frac{dN_p}{d\hat{z}^*} = \int_o^{2\pi} p^* \cos\hat{\theta}\, r_o^*(\hat{z}^*)\, d\theta \tag{17}$$

In terms of the coefficient of pressure

$$Cp = \frac{2(\hat{p}^* - \hat{p}_\infty)}{\hat{\rho}V^2} \tag{18}$$

and the sectional coefficient

$$c_{n,p} = \frac{2\,\frac{dN_p}{d\hat{z}^*}}{\hat{\rho}V^2 d} \tag{19}$$

$$c_{n,p}(\hat{z}) = \frac{1}{2}\int_o^{2\pi} \hat{C}_p(\hat{\theta},\hat{z}) \cos\hat{\theta}\, r_o(\hat{z})\, d\hat{\theta} \tag{20}$$

In two dimensional unsteady flow, let the portion of D(t) due to pressure be

$$D_p(t) = \int_o^{2\pi} p^* \cos\theta\, a^*(t^*)\, d\theta \tag{21}$$

In terms of the coefficient of pressure as in equation (12) and the

coefficient of pressure drag

$$C_{D,p} = \frac{2D(t^*)}{\rho U^2 (2\tilde{a})} \tag{22}$$

$$C_{D,p} = \frac{1}{2}\int_0^{2\pi} C_p \cos\theta \; a(t) \; d\theta \tag{23}$$

From equation (2) and the pressure contribution to equation (16),

$$\hat{C}_p(\hat{\theta},\hat{z}) = C_p(\theta,t) \sin^2\alpha \tag{24}$$

However, as is seen in the following section, this comparison can only be made qualitatively.

3.0 Two Dimensional Unsteady Separated Flow

3.1 General Concepts

The problem is to find the flow field induced by a circular cylinder of time-varying radius in a uniform stream of a viscous incompressible fluid (Figure 2b). The results are to be applied to predict the forces and moments of a body in a three dimensional steady flow field.

The flow field is that of a uniform flow with no body present for $t < 0$. At $t = 0$ a circular body appears at the origin with a radius $a(t)$ such that $a(0) = 0$. During the initial stages a boundary layer (assumed to be laminar) is formed on the circular cylinder. At later times the boundary layer separates from the cylinder, creating vorticity in the flow field immediately after the cylinder. Thus a wake is formed.

In previous work employing the unsteady cross flow with a body of revolution (references 11-23), the two dimensional unsteady solution was derived from a direct use of experimental data or the use of inviscid solutions with ad hoc experimental data to describe the viscous effects. Of note is the work of reference 17 which used the finite difference approach for the two dimensional unsteady problem.

The approach in the present work is unique in that the viscous element, the primary mechanism being the separation of an unsteady boundary layer, is included without resorting to a finite difference approximation to the complete Navier-Stokes equations nor to ad hoc experimental data. This approach can be described as follows:

The problem at early times is sometimes referred to as the cone problem for which no solution exists. It will be approximated by the small time analytical solution (since numerical integration follows, an analytical solution is required for initial conditions) for a circular cylinder of constant radius impulsively started from rest in a viscous incompressible fluid (reference 32). Since the latter can be achieved experimentally by plunging a circular rod into a flowing stream, this approximation is valid for a blunt nosed three dimensional body.

At later times, the solution is obtained by using the technique employed in other work in obtaining the solution for large times for a circular cylinder of <u>constant radius</u> impulsively started from rest (this work will be referred to as "the constant-radius-solution"), and modifying it for a time-varying radius.

The problem for a constant radius cylinder which has received a great amount of attention, is considered a classical problem in separated flow (reference 33). There have been two primary approaches: a solution to the Navier-Stokes equation in finite difference form (reference 34) and a purely inviscid solution (references 14,15). The latter while simpler still requires a computer and must employ empiricism for the separation phenomenon, a viscous action.

The approach adopted in the constant-radius-solution was to use the computer with known solutions (and matching different solutions based upon the physics of the flow field) while retaining viscous phenomena. This approach has succeeded except for the case of the two dimensional unsteady boundary layer where a finite-difference solution was required.

(An approach midway between a finite difference approximation to the Navier-Stokes equation and the model used here is the work of Wu (reference 5)(which did not use unsteady cross flow concepts). The difference is that Wu solved the Navier-Stokes equations in the wake alone while here a set of point vortices was used. Wu's model, while better theoretically, has not been successful at the values of Reynold's numbers used here).

The particulars of the approach of the constant-radius-solution are as follows (see Figure 4): For the time period during which the cylinder moves about a third of its radius the boundary layer is fully attached with classical potential flow outside. Starting at some time before separation, the flow field is given as the

unseparated time dependent boundary layer solution (reference 32), evaluated at this time, as driven by the classical potential flow about the cylinder. The solutions for the laminar boundary layer for later times are then obtained by numerical integration of the boundary layer equations employing Hall's scheme (reference 35). With succeeding times, the boundary layer separates starting at the rear stagnation point and the point of separation moves upstream. At the point of separation, the vorticity flux across the boundary layer is found and during a time Δt, corresponding to the time of integration of the boundary layer, this flux is summed up and represented by a point vortex. This point vortex is convected downstream and its effect is modified by diffusion. Thus, the wake is formed of these point vortices superimposed on the original potential flow. The wake grows, being continually fed with vorticity by the separating boundary layer, while outside of the wake and the boundary layer, irrotational flow exists. This situation continues until the steady state region is attained. Physically a rigorous steady state is never achieved due to instabilities in the wake and mathematically this may only be attained in infinite time. The work of the constant-radius-solution reveals the neighborhood of the steady state is achieved in a finite time (Figure 5) but for its present use, $0 < t < (df/\tilde{a}) \tan \alpha$, the steady state region does not enter.

It is to be noted that the no-slip condition is satisfied on the portion of the cylinder covered by the boundary layer but not on the remaining portion. The wake model as depicted above while

reducing the surface speed of potential flow is not sufficient to yield a surface speed sufficiently less than free stream speed to approximate to a no-slip condition. Thus there is postulated a shear layer on the rear of the cylinder, similar to a boundary layer but with a rotational outer flow, to satisfy no-slip. This rear shear layer may separate, creating vorticity in the wake of the sign opposite to that shed by the boundary layer separation.

For the present problem, the above physical situation is modified by the presence of a time varying radius a(t).

With this approach the flow field is decomposed into a set of sub-flow-fields and their interactions. The governing equations and their solution are given in the following.

3.2 Outer Flow

The flow outside the boundary layer rear shear layer (see Figure 4) is assumed to be the classical potential flow (uniform flow and source and doublet at origin) over a cylinder plus the potential flow induced by a set of point vortices.

In terms of the non-dimensional quantities $[x,y,t] = [x^*/\tilde{a}, y^*/\tilde{a}, Ut^*/\tilde{a}]$, $r = r^*/\tilde{a}^*$, $\Phi + i\,\Psi = (\Phi^* + i\Psi^*) / U\tilde{a}$, $\omega = \tilde{a}\,\omega^*/U$, $\Gamma = \Gamma^*/U\tilde{a}$, the equations for the outer flow are

$$
\begin{aligned}
&\text{DE} \quad \Delta\Psi(x,y,t) = \omega(x,y,t) \\
&\text{IC} \quad t = 0 \quad \Psi = y \\
&\text{BC} \quad 1) \quad r = a : \Psi = -a\mathring{a}\theta \\
&\qquad\quad 2) \quad r \to \infty : \Psi \to y
\end{aligned}
\tag{25}
$$

where $\omega(x,y,t) = \sum_{\beta} \Gamma_{\beta k}\, \delta(x-x_{\beta k})\, \delta(y-y_{\beta k})$

(δ being the delta function) such that $\int\int \omega dS = \sum_{\beta} \Gamma_{\beta k}$.

The $\omega(x,y,t)$ arises from vorticity created by the separation of the boundary and rear shear layers.

The solution is

$$w = \Phi + i\Psi = z + \frac{a^2}{z} - a\dot{a} \log z + i \sum_{\beta} \frac{\Gamma_{\beta k}}{2\pi} \log \frac{(z - z_{\beta k})z}{\left(z - \frac{a^2 z_{\beta k}}{|z_{\beta k}|^2}\right) z_{\beta k}} \tag{26}$$

where

$$z = x + iy = re^{i\theta}$$

$$z_{\beta k} = x_{\beta k} + iy_{\beta k} = \ell_{\beta k} e^{i\theta_{\beta k}}$$

$$z - z_{\beta k} = (x-x_{\beta k}) + i(y-y_{\beta k}) = r_{1\beta k} e^{i\theta_{1\beta k}}$$

$$z - \frac{a^2 z_{\beta k}}{|z_{\beta k}|^2} = x - \frac{a^2 x_{\beta k}}{\ell^2_{\beta k}} + i\left(y - \frac{a^2 y_{\beta k}}{\ell^2_{\beta k}}\right) = r_{2\beta k} e^{i\theta_{2\beta k}}$$

such that when $|z| = a$, $r_{2\beta k} = a\, r_{1\beta k}/\ell_{\beta k}$ and $\Psi = 0$.

Now

$$\frac{dw}{dz} = -\tilde{u}^\circ + i\tilde{v}^\circ = e^{-i\theta}(-v^\circ + iu^\circ) \tag{27}$$

The form of the equations used in the computations, as in Part II, are obtained as follows; since

$$\frac{dw}{dz} = 1 - \frac{a^2}{z^2} - \frac{a\dot{a}}{z} + i \sum_{\beta} \frac{\Gamma_{\beta k}}{2\pi} \left\{ \frac{1}{z - z_{\beta k}} - \frac{1}{z - \frac{a^2 z_{\beta k}}{|z_{\beta k}|^2}} + \frac{1}{z} \right\}$$

then

$$-\tilde{u}^\circ + i\tilde{v}^\circ = 1 - a^2 \frac{[x^2 - y^2 - 2ixy]}{r^4} - a\dot{a} \frac{(x - iy)}{r^2}$$

$$+ \sum_{\beta} \frac{\Gamma_{\beta k}}{2\pi} \left\{ \frac{y - y_{\beta k} + i(x - x_{\beta k})}{r_{1\beta k}^2} - \frac{y - \frac{a^2 y_{\beta k}}{\ell^2_{\beta k}} + i \left(\frac{x - a^2 x_{\beta k}}{\ell^2_{\beta k}} \right)}{r_{2\beta k}^2} \right.$$

$$\left. + \frac{y + ix}{r^2} \right\} \qquad (28)$$

and

$$-v^\circ + iu^\circ = e^{i\theta} - \frac{a^2 e^{-i\theta}}{r^2} - \frac{a\dot{a}}{r} + ie^{i\theta} \sum_{\beta} \frac{\Gamma_{\beta k}}{2\pi} \left\{ \frac{e^{-i\theta_{1\beta k}}}{r_{1\beta k}} - \frac{e^{-i\theta_{2\beta k}}}{r_{2\beta k}} + \frac{e^{-i\theta}}{r} \right\}$$

(29)

Since

$$e^{-i\theta_{1\beta k}} = \frac{1}{r_{1\beta k}} [x - x_{\beta k} - i(y - y_{\beta k})] = \frac{re^{-i\theta} - \ell_{\beta k} e^{-i\theta_{\beta k}}}{r_{1\beta k}}$$

$$e^{-i\theta_{2\beta k}} = \frac{1}{r_{2\beta k}} \frac{x - a^2 x_{\beta k}}{\ell^2_{\beta k}} - i \left(y - \frac{a^2 y_{\beta k}}{\ell^2_{\beta k}} \right) = \frac{re^{-i\theta} - \frac{a^2 e^{-i\theta_{\beta k}}}{\ell_{\beta k}}}{r_{2\beta k}}$$

$$-v^\circ + iu^\circ = e^{i\theta} - \frac{a^2 e^{-i\theta}}{r^2} - \frac{a\dot{a}}{r} + i \sum_\beta \frac{\Gamma_{\beta k}}{2\pi} \left\{ \frac{r-\ell_{\beta k} e^{i(\theta-\theta_{\beta k})}}{r_{1\beta k}^2} - \frac{r - \frac{a^2}{\ell_{\beta k}} e^{i(\theta-\theta_{\beta k})}}{r_{2\beta k}^2} + \frac{1}{r} \right\} \tag{30}$$

such that when $r = a$,

$$-v_\circ^\circ + iu_\circ^\circ = -\dot{a} + i\, 2 \sin\theta + i \sum_\beta \frac{\Gamma_{\beta k}}{2\pi} \left\{ \frac{a^2-\ell_{\beta k}^2}{a\, r_{1\beta k}^2} + \frac{1}{a} \right\} \tag{31}$$

Non-dimensionalizing the pressure as $p = 2p^*/\rho U^2$, the Bernoulli equation is

$$-\Phi_{,t} + \frac{(u_\circ^{\circ 2} + v_\circ^{\circ 2})}{2} + \frac{p}{2} = f(t) \tag{32}$$

Then since

$$\Phi = \cos\theta\left(r + \frac{a^2}{r}\right) - a\dot{a} \log r - \sum_\beta \frac{\Gamma_{\beta k}}{2\pi} \{\theta_{1\beta k} - \theta_{2\beta k} + \theta - \theta_{\beta k}$$

$$\Phi_{,t} = \frac{2a\dot{a}}{r} \cos\theta - \frac{d}{dt}(a\dot{a}) \log r - \sum_\beta \frac{\Gamma_{\beta k}}{2\pi} \{\dot{\theta}_{1\beta k} - \dot{\theta}_{2\beta k} - \dot{\theta}_{\beta k}\} \tag{33}$$

where

$$\dot{\theta}_{1\beta k} = \frac{-\dot{y}_{\beta k}(x-x_{\beta k}) + \dot{x}_{\beta k}(y-y_{\beta k})}{r_{1\beta k}^2}$$

$$\dot{\theta}_{2\beta k} = \left\{ - \frac{d}{dt}\left(\frac{a^2 y_{\beta k}}{\ell_{\beta k}^2}\right) \cdot \frac{x-a^2 x_{\beta k}}{\ell_{\beta k}^2} + \frac{d}{dt}\left(\frac{a^2 x_{\beta k}}{\ell_{\beta k}^2}\right) \cdot \frac{y-a^2 y_{\beta k}}{\ell_{\beta k}^2} \right\} \left(\frac{1}{r_{2\beta k}^2}\right)$$

$$\dot{\theta}_{\beta k} = \frac{[\dot{y}_{\beta k} x_{\beta k} - \dot{x}_{\beta k} y_{\beta k}]}{\ell_{\beta k}^2}$$

Since

$$\lim_{r\to\infty} \Phi_{,t} = \sum_{\beta} \frac{\Gamma_{\beta k}}{2\pi} \dot{\theta}_{\beta k} - \frac{d}{dt}(a\dot{a}) \lim_{r\to\infty} \log r,$$

$$f(t) = -\sum_{\beta} \frac{\Gamma_{\beta k}}{2\pi} \dot{\theta}_{\beta k} + \frac{1}{2} + \frac{p_\infty}{2} + \frac{d}{dt}(aa) \lim_{r\to\infty} \log r$$

such that the pressure coefficient on the surface

$$C_p \equiv p - p_\infty = \left[2\Phi_{,t}\Big|_{r=a} - (u_o^2 + v_o^2) + 1\right]$$

$$- 2 \sum_{\beta} \frac{\Gamma_{\beta k}}{2\pi} \dot{\theta}_{\beta k} + 2 \frac{d}{dt}(a\dot{a}) \lim_{r\to\infty} \log r \qquad (34)$$

Considering only those terms contributing to drag

$$C_p = 4\,\dot{a}\cos\theta - 2 \sum_{\beta} \frac{\Gamma_{\beta k}}{2\pi} \left[\dot{\theta}_{1\beta k} - \dot{\theta}_{2\beta k}\right]_{r=a}$$

$$- \left[2\sin\theta + \sum_{\beta} \frac{\Gamma_{\beta k}}{2\pi} \left[\frac{a^2 - \ell_{\beta k}^2}{a^2 r_{1\beta k}^2 (r=a)} + \frac{1}{a}\right]\right]^2 \qquad (35)$$

Note that the term in equation (34), $\lim_{r\to\infty} \log r$, precludes an absolute determination of C_p.

3.3 Boundary Layer

The unsteady two dimensional Navier-Stokes equations in polar coordinates are (nondimensionalizing as in the outer flow and with $\tau = 2\tau^*/\rho U^2$),

$$\text{DE} \qquad \frac{(rv)_{,r}}{r} + \frac{u_{,\theta}}{r} = 0$$

$$\frac{Du}{Dt} + \frac{uv}{r} = -\frac{p_{,\theta}}{2r} + \delta^2\left[L[u] + \frac{2v_{,\theta}}{r^2}\right]$$

$$\frac{Dv}{Dt} - \frac{u^2}{r} = -\frac{p_{,r}}{2} + \delta^2\left[L[v] - \frac{2u_{,\theta}}{r}\right] \tag{36a}$$

where $$\frac{D}{Dt} = (\ )_{,t} + \frac{u(\ )_{,\theta}}{r} + v(\ )_{,r}$$

$$L[\ ] = (\ )_{,rr} + \frac{(\ )_{,r}}{r} - \frac{(\ )}{r^2} + \frac{(\ )_{,\theta\theta}}{r^2}$$

with $$\omega = \frac{(ru)_{,r}}{r} - v_{,\theta,r} \ ; \quad \tau = 2\delta^2 u_{,r}$$

and where $$\delta^2 = \frac{1}{Re_{2DUS}} = \frac{\nu}{U\tilde{a}}$$

$$\text{IC} \qquad t = t_o > 0; \quad u = f(r,\theta), \quad v = g(r,\theta) \tag{36b}$$

and boundary conditions at the surface

$$\text{BC} \qquad r = a(t): \quad u = 0, \quad v = \dot{a} \tag{36c}$$

Defining the inner variables

$$[\bar{u},\bar{v}] = \left[u, \frac{(v - \frac{a\dot{a}}{r})}{\delta}\right] , \quad [\bar{\theta},\bar{r},\bar{t}] = \left[\theta, \frac{r - a(t)}{\delta}, t\right] \tag{37}$$

substituting into equations (36) and letting $\delta \to 0$, one obtains the (laminar) boundary layer equations.

$$\text{DE} \qquad \frac{\bar{u}_{,\bar{\theta}}}{a} + \bar{v}_{,\bar{r}} = 0$$

$$\bar{u}_{,\bar{t}} + \bar{v}\,\bar{u}_{,\bar{r}} + \frac{\bar{u}\bar{u}_{,\theta}}{a} - \frac{\dot{a}\bar{r}\bar{u}_{,\bar{r}}}{a} + \frac{\dot{a}}{a}\bar{u} = -\frac{p_{,\bar{\theta}}}{2a} + \bar{u}_{,\bar{r}\bar{r}}$$

$$0 = -p_{,\bar{r}}\,, \quad \omega = \frac{\bar{u}_{,\bar{r}}}{\delta}\,, \quad \tau = 2\,\delta\,\bar{u}_{,\bar{r}} \tag{38a}$$

with

$$\text{IC} \qquad t = t_o\text{:}\ \ \bar{u} = f'(\bar{r},\bar{\theta}),\ \bar{v} = g'(\bar{r},\bar{\theta}) \tag{38b}$$

$$\text{BC} \qquad 1)\ \ \bar{r} = 0\text{:}\ \ \bar{u} = \bar{v} = 0$$

$$2)\ \ \bar{r} \to \infty\text{:}\ \ \bar{u} \to u_o^{\circ}(\bar{\theta},\bar{t}) \tag{38c}$$

BC2) being derived from the matching concept.

As such the Hall scheme of integration (reference 38) is not applicable. If the transformation is made,

$$u^i = a\bar{u}$$

$$v^i = \bar{v} - \frac{\dot{a}}{a}\bar{r} \tag{39}$$

then the problem is

$$\text{DE} \qquad \frac{u^i{}_{,\theta}}{a^2} + v^i{}_{,\bar{r}} = -\frac{\dot{a}}{a}$$

$$u^i{}_{,t} + \frac{u^i u^i{}_{,\bar{\theta}}}{a^2} + v^i u^i{}_{,\bar{r}} = (au_o^{\circ})_{,t} + (au_o^{\circ})\frac{(au_o^{\circ})_{,\bar{\theta}}}{a^2} + u^i{}_{,\bar{r}\bar{r}} \tag{40a}$$

$$\omega = \frac{u^i{}_{,\bar{r}}}{a\delta}\,, \qquad \tau = \frac{2\delta u^i{}_{,\bar{r}}}{a}$$

$$\text{IC} \qquad t_o = t_o\text{:}\ \ u^i = f''(\bar{r},\bar{\theta}),\ v^i = g''(\bar{r},\bar{\theta}) \tag{40b}$$

BC 1) $\bar{r} = 0$: $u^i = v^i = 0$

2) $\bar{r} \to \infty$: $u^i \to a u_o^i(\bar{\theta}, t)$

where $p_{,\bar{\theta}}$ has been evaluated at $\bar{r} \to \infty$ by virtue of $p_{,\bar{r}} = 0$ (40c)

Except for the source term "$-\dot{a}/a$" in the continuity equation and the factor "$1/a^2$" multiplying the $(\ )_{,\bar{\theta}}$ terms, the form of the equation is identical with the classical equations. Thus modifying the Hall method by the inclusion of a source term and modifying finite difference in $\bar{\theta}$ terms by the factor $1/a^2(t)$, the Hall scheme is applicable.

3.4 Boundary Layer Separation Region

The numerical integration scheme used to obtain solutions to the unsteady two dimensional laminar boundary layer equations, being based upon boundary layer approximations, is not valid at the separation region. In addition, a definition of the separation region in unsteady flow is a controversial issue (references 36-38). The approach used here is the classical one of carrying over the definition of separation for steady flow, i.e. $\tau = 0$, to unsteady flow.

Employing $\tau = 0$ as the definition of separation, the numerical scheme used did predict a meaningful separation region (based upon the constant-radius solution). In the scheme actually used the particular grid point on the cylinder immediately upstream of the point at which $\tau \leq 0$ was used to define the separation point, θ_s.

3.5 Boundary Layer - Outer Flow Interface

Let the separation point of the boundary layer be $\theta_s(t_k) \equiv \theta_{sk}$ where t_k are the discrete times of the numerical integration. Physically,

at this point, the vorticity created in the boundary layer passes into the outer flow. This is found as follows:

The vorticity flux across the section of the boundary layer at θ_{sk} is

$$\Gamma_{,t}(t_k) = \int_a^\infty \omega\, u\, dr \tag{41}$$

Since $\omega = \bar{u}_{,\bar{r}}/\delta$, $u = \bar{u}$ and $dr = \delta d\bar{r}$ in the boundary layer

$$\Gamma_{,t} = \int_o^\infty \bar{u}_{,\bar{r}}\, \bar{u}\, d\bar{r} = \frac{\bar{u}^2}{2}\Big|_o^\infty = \frac{u_o^{\circ 2}}{2} \tag{42}$$

using no-slip.

During the period $t_k < t < t_{k+1}$, this vortex flux is summed into one point vortex of strength,

$$\Gamma_{\beta k}\Big|_{\beta=k} = \Gamma_{,t}\,(t_k)\,\Delta t_k; \quad \Delta t_k = t_{k+1} - t_k \tag{43}$$

where β denotes the point vortex label.

Considering this vortex to be in the outer potential flow, its images are born at the same time. The surface velocity due to this just born point vortex and its images is $-\Gamma_{\beta k}/\pi m_k$ where m_k is its distance from the surface of cylinder into the flow. If this velocity is used to cancel the velocity at the surface induced by the outer flow minus this new born vortex, then its position is

$$m_k = \frac{|\Gamma_{\beta k}|}{\pi |u_o^\circ|} = \frac{|u_o^\circ|\,\Delta t_k}{2\pi} \tag{44}$$

where $|u_o^\circ|$ is induced by outer flow minus the new born vortex.

Alternatively, this can be interpreted as a condition on the Δt_k of numerical integration of the boundary layer; i.e.

$$\Delta t_k = \frac{2\pi m_k}{|u_o^o|} \tag{45}$$

where now $m_k \sim 1/\sqrt{Re_{2DUS}}$, of the order of the boundary layer thickness (found, for example, by the first moment of the vorticity distribution).

Now this argument must be compatible with the constraint on Δt_k imposed by the workability of the numerical integration scheme employed in the boundary layer.

A Δt_k found by equation (45) was used successfully in early runs but it was found that increasing the Δt_k over this value lead to the same results with a savings in computer time.

Thus the final results used a Δt_k which was such that i) The numerical integration scheme for the boundary layer equations was workable, and ii) the resulting m_k, as given by equation (44), was "in" the boundary layer which was assumed to be much less than the radius of the cylinder; i.e. $m_k < 0.1a$.

3.6 Rear Shear Layer

The mathematical model described so far leaves the satisfaction of the no-slip condition at the rear of the cylinder in the absence of the boundary layer (i.e., where the separation point is upstream) to the velocity induced by the array of free shed point vortices. These induce a velocity on the surface counter to that given by uniform flow over a cylinder. However, the counter-velocity sometimes

exceeds the latter velocity and the no-slip condition is not satisfied.

To satisfy the no-slip condition, the existence of a rear shear layer is postulated. The rear shear layer is similar to a boundary layer except that the outer flow is rotational. Since there is no theory for such a rear shear layer (time dependent) and since its prime contribution is the production of vorticity, then it is postulated:

a) there exists a rear shear layer when $|u_o^\circ| > 0.1$.

For $0 < \theta < \pi$ (with similar equations for $\pi < \theta < 2\pi$),

b) the separation point of rear shear layer is given as a function of the boundary layer separation point location by means of the following: (see Figure 6)

$$\frac{\theta_s^f - \theta_m^f}{\theta_o - \theta_m^f} = \frac{\theta_m^r - \theta_s^r}{\theta_m^r - \theta_o} \tag{46}$$

Thus the location of the separation region of the rear shear layer is primarily a function of the boundary layer separation location.

c) A point vortex is born at θ_s^r of strength

$$\Gamma_{r\beta k} = \Gamma_{,t} \Delta t_k = \frac{u_o^{\circ 2} \Delta t_k}{2}$$

$$\beta = k$$

at a point $[r,\theta] = [a_k + m_{rk}, \theta_{sk}^r]$ (47)

where $m_{rk} = \frac{|u_o^\circ| \Delta t_k}{2\pi}$

only if $\frac{d\theta_{sk}^r}{dt} \geq 0$

d) N($\leq$ 5) point vortices are replaced by one point vortex of strength

$$\Gamma = \sum_{k=1}^{N} \Delta t_k \left(\frac{u_o^{\circ 2}}{2}\right)_k < 0.1 \qquad (48)$$

at position $m_{rk} = \frac{\Gamma}{\pi \langle u_o^\circ \rangle} < 0.1$

where $\langle u_o^\circ \rangle$ = average of u_o° at θ_s^f .

This operation is used to reduce computer time and is allowable since one just born point vortex is of small strength (compared with one born from the boundary layer) and the separation point, as defined above, undergoes oscillation. Thus the operation is an averaging and coalescing mechanism).

3.7 Wake-Vortex Convection

The sum of point vortices in the outer flow define the wake. Each point vortex, labeled β, moves with the cartesian velocity components of the outer flow. Thus

$$x_{\beta k+1} = x_{\beta k} + \Delta t_k \, \tilde{u}^\circ(x_{\beta k}, y_{\beta k}, t_k)$$

$$y_{\beta k+1} = y_{\beta k} + \Delta t_k \, \tilde{v}^\circ(x_{\beta k}, y_{\beta k}, t_k) \qquad (49)$$

where the contribution to $[\tilde{u}^\circ, \tilde{v}^\circ]$ of the point vortex at $[x_{\beta k}, y_{\beta k}]$ is omitted.

3.8 Wake-Vortex Diffusion

A point vortex undergoes both convection and diffusion. Convection is treated in the manner just described. Diffusion is handled as follows: for an isolated stationary point vortex, the governing equation is the diffusion equation with the potential solution as the initial condition. Thus following reference 39,

$$\text{DE} \qquad \omega_{,t} = \delta^2(\omega_{,rr} + \frac{\omega_{,r}}{r}); \; r > 0$$

$$t = 0: \qquad = \frac{\Gamma_o}{2\pi}, \quad r = 0 \qquad (50)$$

$$= 0, \quad r > 0$$

The solution is, with $\delta^2 = 1/\text{Re}(\equiv 1/\text{Re}_{2\text{DUS}})$

$$\omega(r,t) = \frac{\Gamma_o}{4\pi t} \; \text{Re} \; e^{-\text{Re} \; r^2/4t} \qquad (51)$$

with an induced velocity distribution (see Figure 7).

$$u(r,t) = \frac{1}{2\,r} \int_o^{2\pi}\int_o^r \omega \; r \; dr \; d_\theta = \frac{\Gamma_o}{2\pi r}(1 - e^{-\text{Re} \; r^2/4t}) \qquad (52)$$

The viscous core radius $r_c(t)$ is defined as the distance from the center to the point at which u is a maximum. From the above equations this is

$$r_c(t) = \sqrt{\frac{5.04t}{\text{Re}}} \qquad (53)$$

For $R_e = 4.10^4$

$$r_c(t) = 0.0112\sqrt{t} \qquad (54)$$

Then the potential flow solution for a point vortex is assumed valid for $r > r_c$ (see Figure 7).

The concept of a core radius r_c is used in two applications.

Surface pressure. If a point vortex is located in the neighborhood of the surface of the cylinder, a potential flow velocity distribution would induce a high velocity at the surface which would imply a peak in the pressure distribution on the surface.

Approach of Two Point Vortices. If two vortices are close together anywhere in the flow, the potential flow velocity distribution would induce local high velocities.

(Although peaks have been found experimentally, their small scale property is not compatible with the present mathematical model).

Both effects are resolved by the diffusion action which reduces the potential flow velocity in the neighborhood of the point vortex.

One way to resolve this is to program an r_c as a function of the life-time of a point vortex via equation (53) and use the velocity distribution (see Figure 7).

$$u = 0; \quad r < r_c(t)$$

$$= \frac{\Gamma}{2\pi r} ; \; r > r_c(t) \text{ (potential flow)} \qquad (55)$$

However, the employment of r_c as a function of t is insufficient within the present mathematical model which employs an approximation to the convection of the vortices as in equation (49) [i.e. $\Delta x \sim \Delta t$]. Thus the errors inherent in this convection approximation could place a point vortex sufficiently close to the surface or another point

vortex such that r_c for a small times is insufficient to rule out high local velocities.

In lieu of the r_c as a life-time function, the values of $r_c = .05$ was used throughout. This is an average value of the life-time function, compatible with a large number of vortices, and is sufficient to rule out singularities.

3.9 Wake-Vortex Coalescence

The wake consists of a set of point vortices, the number of which grows with time. To reduce the computing time, the number is reduced at certain times by means of coalescing pairs of vortices into one vortex. The criteria are that the velocity field induced by the new vortex is equivalent to that induced by the original pair, and the times at which this operation is applied are those times at which the number of vortices is overly sufficient to yield an acceptable flow field and so a reduction of the number does not destroy the intrinsic structure of the wake (references 40 and 41).

The operation is as follows: two point vortices of strengths Γ_1 and Γ_2, at $[x_1,y_1]$ and $[x_2,y_2]$ respectively are replaced by one point vortex of strength Γ_3 at $[x_3,y_3]$ where

$$\Gamma_3 = \Gamma_1 + \Gamma_2$$

$$x_3 = \frac{(|\Gamma_1|x_1 + |\Gamma_2|x_2)}{(|\Gamma_1| + |\Gamma_2|)} \qquad (56)$$

$$y_3 = \frac{(|\Gamma_1|y_1 + |\Gamma_2|y_2)}{(|\Gamma_1| + |\Gamma_2|)}$$

(absolute signs to coalesce vortices of opposite sign). Then, if $(x_2 - x_1)r_1$ and $(y_2 - y_1)/r_1$, $\left[r_i^2 = (x - x_i)^2 + (y - y_i)^2 \;; i = 1,2,\right]$ are of order $\varepsilon << 1$ then

$$\tilde{u}_3 = (\tilde{u}_1 + \tilde{u}_2)(1 + 0(\varepsilon))$$
$$\tilde{v}_3 = (\tilde{v}_1 + \tilde{v}_2)(1 + 0(\varepsilon)) \qquad (57)$$

3.10 Wake-Vortex Stability

For early times the flow field consists of an outer potential flow over a cylinder with free point vortices at the rear and an inner flow (the boundary layer and a possible rear shear layer) with all solutions symmetric about y = 0. It is known that this structure is unstable and asymmetry arises (references 42,43). This is usually obtained by supplying a small perturbation to the point vortex array and having the system determine the new stable asymmetric structure.

However, for the times involved in the application of the theory, there would be negligible asymmetry. Thus to reduce computer time, symmetric wakes were assumed.

3.11 Vortex Flux Parameter

It was found that the accuracy of the resulting force and moment data in comparison with experimental data (see Section 5.0) could be improved in certain cases by reducing the vorticity in the wake by a factor $(1-\sigma)100\%$ from the value actually produced by the separation of the boundary and rear shear layers. For the two tests performed (see Section 4.0) no reduction was required for the closed-ended ellipsoid (i.e. $\sigma = 1$) but a reduction of 40% improved the results for the open-ended ogive-cylinder (i.e. $\sigma = 0.6$).

This is the only empirical factor in the technique. Its role may be viewed as similar to the eddy viscosity in turbulence; i.e. empiricism arises in the absence of complete theoretical understanding. In this situation, there is no theoretical derivation of the equivalence underlying the unsteady cross flow analogy. Further light would be shed on this with further testing.

This factor is not related to the reduction in wake vorticity from that produced by the boundary layer alone in the classical problem of a circular cylinder of constant radius impulsively started from rest (see references 44,45). In earlier work with the constant-radius-solution, treating this problem, it was found that the rear shear layer effectively accounted for this reduction by introducing vorticity of sign opposite to that introduced by the boundary layer.

3.12 Drag

At representative times, the drag is computed in equations (11), (12), (13) and (14). The pressure is obtained from the Bernoulli equation, equation (35) and the shear stress from the boundary layer solution $\tau = 2\delta\ \bar{u},_{\bar{r}} = 2\delta\ \bar{u}(\Delta\bar{r},\theta t)/\Delta\bar{r}$ by virtue of the no-slip condition.

Within a completely inviscid model, the drag may be obtained using the vortex-impulse concept or Lagally's theorem. However, drag is obtained herein by pressure and shear integration since the wake model, while primarily inviscid, does have diffusive effects and, more importantly, the surface pressures are of interest in establishing the equivalence property. Computational times are of the same order.

4.0 Applications

4.1 Test Data

The foregoing theory will be applied to two bodies for which experimental data is available. The first test case is that of an ogive-cylinder with a blunt base at subsonic speeds (reference 6). The second test case is that of an ellipsoid of revolution at low speeds (reference 7). The latter presents a severe test in that the geometry is that of a closed-ended body such that for all angles of attack, there may not exist any boundary layer on the aft end. The theory as presented so far does not cover this eventuality (although it may easily be extended). However, even without this specific capability, meaningful results can be obtained.

Test Case 1: Ogive-Cylinder (Reference 6)

Geometry and Test Condition

$$r_o^*(\hat{z}^*) = d\left[\left(\frac{\ell_n}{d}\right)^2 - \frac{1}{4}\right] - d\left[\left(\frac{1}{4} + \left(\frac{\ell_n}{d}\right)^2\right)^2 - \left(\frac{\hat{z}^*}{d} - \frac{\ell_n}{d}\right)^2\right]^{1/2}; \quad 0 \le \hat{z}^* \le \ell_n$$

$$= \frac{d}{2}; \quad \ell_n \le \hat{z}^* \le \ell$$

where ℓ_n is the nose (ogive) length.

$\ell = 1.282$ m, $d = .1194$ m, $\ell_n = 3d$, $f = \frac{\ell}{d} = 10.74$

$Re_{3DS} = 4.7 \times 10^6$, $M = 0.3$

$0 \le \alpha \le 24°$

$\tilde{a} = \frac{d}{2} = .0597$ m

Inviscid Theory Results

Slender Body $\quad c_n = \frac{\pi\alpha}{f} r_o \frac{dr_o}{d\hat{z}}$

$$C_N = 2\alpha$$

$$C_M = 2\alpha \left[\frac{\text{Vol.}}{\ell S_B} - 1\right]$$

Test Case #2: Ellipsoid of Revolution (Reference 7)

Geometry and Test Conditions

$$r_o^*(\hat{z}^*) = \left(\frac{1}{f}\right) \sqrt{\hat{z}^*(\ell - \hat{z}^*)} \; ; \quad 0 \le \hat{z}^* \le \ell$$

$\ell = 0.6096$ m., $d = 0.1524$ m., $f = \frac{\ell}{d} = 4$

$V = 12.192$ m./s., $\hat{\rho} = 1.226$ kg./m.^{3}, $q = \frac{\hat{\rho}V^2}{2} = 91.924$ newt./m.^{2}

$\nu = 14.957\ 10^{-6}$ m^2/sec., $Re_{3DS} = 4.97 \times 10^5$

$0 \le \alpha \le 20°$

$$\tilde{a} = \frac{1}{\ell} \int_o^{\ell} r_o^*(\hat{z}^*)\, d\hat{z}^* = .05913 \text{ m.}$$

Inviscid Theory Results

Potential Flow $\quad c_n = f_1 f_2 \cos^2\beta \sin 2\alpha$

where $\quad$ where $\quad f_1 = \frac{\pi}{2}\left(\frac{1}{2} - \hat{z}\right)$, $f_2 = 1.0062$

$$\cos^2\beta = 1 + \frac{\left(\hat{z} - \frac{1}{2}\right)^2}{16\hat{z}(1 - \hat{z})}$$

$$C_N = 0, \quad C_{M,1/2} = .5185 \sin 2\alpha$$

Slender Body $\quad c_n = \frac{\pi}{2}\left(\frac{1}{2} - \hat{z}\right) \sin 2\alpha$

$$C_N = 0, \quad C_{M,1/2} = \frac{2 \sin 2\alpha}{3}$$

4.2 Boundary Layer Integration Parameters

The following parameter values were used:

$$\Delta\bar{r} = .14, \quad \Delta\theta \text{ variable}, \quad \Delta t = .125$$

4.3 Numerical Integration Parameters:

The particular numerical integration sub-routines are to be found in Part II. The sub-routines are such that with a given integrand, less than 2% error is incurred in obtaining the integral.

5.0 Results and Discussion

5.1 General Results

The results of applying the theory to the two test cases are to be found in Figures 8-18.

Primarily the theory yields results capable of describing experimental data at high angles of attack where inviscid theories (potential and slender body) fail (Figures 8 and 14). In achieving this state of data only one element of empiricism, the vortex flux parameter, σ, was used.

5.2 Ogive-Cylinder

Figure 8 shows the basic results, the comparison of the values obtained by this technique and inviscid theory with experimental

data for the normal force and pitching moment. The accuracy of inviscid theory, incapable of describing separation phenomena, decreases rapidly with increase in the angle of attack while the present theory remains valid.

A value of 0.6 was used for the vortex flux parameter, σ, to obtain these curves. There is the potential of increased accuracy in these results through further testing based upon variation of this parameter (see below, in discussion of Figure 10).

Figure 9 presents the basic input data to the curves of Figure 8, the sectional normal force coefficient $c_n(\hat{z},\alpha)$ as a function of the axial station $\hat{z}$. It is noted that for $0 < \hat{z} < 0.3$, inviscid theory suffices. This behavior is pertinent to the discussion (see Section 2.1) of the property of no upstream influence intrinsic to the unsteady cross flow analogy. The flow field relevant to Figure 9 is subsonic which allows for upstream influence and the inviscid theory results contain this property. Yet there is agreement between the two, even at $\alpha = 20°$ where any slender body equivalence principle should not be expected to hold. This behavior lends support to the use of the unsteady cross flow analogy.

For $\hat{z} > 0.3$, inviscid theory predicts $c_n = 0$, while results of employing the unsteady cross flow technique match experimental data. This is a separated region where the use of inviscid theory is obviously invalid.

Figure 10 displays the effect of a change of σ in the $c_n(\hat{z},\alpha)$ vs. $\hat{z}$ data. ($\Delta t = .0625$ was used in these runs while $\Delta t = .125$

was used in the runs of Figures 8 and 9. However, on the basis of early testing based upon Δt variation, the data is relatively insensitive to this change in Δt). Two values of σ were used $\sigma = 0.5$ and $\sigma = 1.0$. The reduction of σ reduced the theoretical results to the neighborhood of the experimental data. An explanation for this behavior lies in the physics of the two dimensional unsteady flow problem. The drag value approaches zero as the wake disappears (D'Alambert's paradox). Thus a reduction in the wake strength reduces drag which is proportional to the sectional normal force. (Note that this argument, based on a cylinder of constant radius, is valid on the aft end of the ogive-cylinder). As a result of this test the value $\sigma = 0.6$ was decided upon.

It is noted that the experimental data was based upon a $Re_{3DS} = V\ell/\nu = 4.73 \times 10^6$ yielding the two-dimensional unsteady flow Reynolds numbers $Re_{2DUS} = U\tilde{a}/\nu = 1.9, 3., 5.7, 7.5,$ and 8.9×10^4 for $\alpha = 5, 10, 15, 20$ and $24°$ respectively (see equation (16)). For a two dimensional circular cylinder in steady flow a Reynolds number of 4.5×10^4 is used as a lower limit for transition and this value is exceeded for $\alpha \geq 15°$. However, the assumption is made that laminar boundary layers exist at all these Reynolds' numbers, including transition values.

Figure 11 indicates typical behavior of the coefficient of pressure on the surface at various axial stations and angles of attack. As noted in the preceding the two-dimensional unsteady pressure distribution yields a logarithmic singularity. However, this term is independent of θ and so a C_p, subject to an arbitrary additive

factor, can be determined. Thus these curves are qualitative. Within this context, the agreement is very good.

Figure 12 presents the separation regions of three dimensional steady flow as obtained by this technique. In the absence of experimental data, these results can only be deemed physically acceptable.

Figure 13 show wake vortex patterns. These present the positions of shed point vortices at one time or axial position and their position at the succeeding time or axial position. Thus the distribution of vorticity and the partial streamline pattern is indicated.

5.3 Ellipsoid of Revolution

The basic result for the ellipsoid, the comparison of the values obtained by this technique and inviscid theory with experimental data for the normal force and pitching moment about the midpoint are presented in Figure 14. In this case the improvement of this technique over inviscid theory is marked since the latter yields $C_N = 0$ (reflecting the closed-end).

These results employed a vortex flux factor of $\sigma = 1.0$ (i.e. no reduction)(see discussion below for Figure 15).

The curves of Figure 14 are a result of the integration of the section normal force coefficient $c_n(\hat{z},\alpha)$ over z. The integrand, $c_n(\hat{z},\alpha)$ is presented in Figure 15 as a function of the axial station $\hat{z}$ at various angles of attack, α. In interpreting these curves as integrands, attention had to be paid to the behavior in the neighborhood of the base. In this region, there is no boundary layer; the tail lies within the wake. As noted earlier the theory as developed thus

far does not handle this situation although the extension can easily be made. And before the computations reach the section of no boundary layer, the radius a(t) may change rapidly (for a closed-ended body such as the ellipsoid) such that very fine integration meshes are required with consequent increase in computer time. Furthermore, the basic assumptions of the two-dimensional unsteady boundary layer solution technique may fail, particularly with regard to the property of no pressure change across the boundary layer.

In lieu of increasing the complexity of the technique, computation was formally stopped at $\hat{z} = 0.9 \boxminus \hat{z}_f$ and at a straight line drawn to complete the curve at $(c_n, \hat{z}) = (0, 1.0)$, a theoretically exact point. Figures 15b and 15c show the differences in behavior for two stopping stations $\hat{z}_f = 0.9$ and 1.0. The latter value, in both cases, departs from the experimental data.

Figures 15b and 15c also show the effect of varying the vortex flux parameter σ. For $\alpha = 10°$ there is little difference but for $\alpha = 20°$ the difference is marked. The behavior in this case is the same as for the ogive cylinder in that a reduction in σ reduces drag which in turn reduces the section normal forces. However, in this case, the physics is not as clear since the corresponding two dimensional unsteady problem is that concerned with a cylinder whose radius is changing rapidly with time. Also, the reduction in vortex flux increases the error as opposed to the situation in the case of the ogive-cylinder.

The experimental data was obtained for a $Re_{3DS} = 4.97 \times 10^5$

yielding the two dimensional unsteady flow Reynold's numbers of $Re_{2DUS} = 3.4, 5.0, 8.36$ and 16.5×10^3 at $\alpha = 4, 6, 10$ and $20°$ respectively (see equation (16)). Based upon two dimensional steady flow, laminar boundary layers should exist.

Figure 16 shows the pressure distribution for $\alpha = 20°$ at various $\hat{z}$. The curve must still be considered as qualitative (i.e. with an arbitrary additive constant). It is to be noted that qualitative agreement is found at $\hat{z} = .72$ but for $\hat{z} > .86$ where the tail is in the wake, even this qualitative agreement is lost.

Figure 17 depicts the regions of separation of a three dimensional steady flow field as determined by this theory compared with that determined by a finite difference solution (reference 46). The agreement is fairly good. Of note are the divergences on the aft windward region but in this region, the particular behavior determined by means of this technique agrees with experimental data (reference 47).

Figure 18 show wake vortex patterns, explained in the ogive-cylinder case.

5.4 Vortex Flux Parameter

As was noted, the value of the vortex flow parameter used was $\sigma = 1.0$ for the ellipsoid and $\sigma = 0.6$ for the ogive-cylinder. The prime difference between the two geometries is at the base: open-ended for the ogive-cylinder and closed-ended for the ellipsoid. Thus the recommendation for use of this technique for an arbitrary body is a value of σ given by

$$\sigma = 1.0 - \frac{0.8 r_o^*(\ell)}{d} , \qquad (58)$$

a linear fit over the two test points.

5.5 Computational Times

The maximum time for computation occurred for the ogive cylinder at an angle of attack of 24°. The time was 45 minutes (on a CDC 6500 at Purdue University). Since the computation time is proportional to the final time of the problem, $(df/\tilde{a}) \tan \alpha$ (see equation (2)), an estimate of computational times required can be given by

$$\text{computational time (min.)} = \frac{24}{\left[\frac{fd}{\tilde{a}} \tan \alpha\right]_{O\text{-}C \text{ at } \alpha = 24^\circ}} \frac{fd}{\tilde{a}} \tan \alpha$$

$$= \frac{2.5\ fd}{\tilde{a}} \tan \alpha$$

However, it is believed that substantial reductions are possible through further work on the basic solution techniques and, to a lesser extent, in the programming.

6.0 Conclusions

The method developed herein employing the unsteady cross flow analogy and a discrete vorticity wake for the prediction of local flow conditions and overall forces and moments on bodies at high angles of attack with large regions of separated flow has been shown to be technically feasible. The method is based upon physical understanding of the flow and does not require a complete finite difference solution to the Navier-Stokes equations.

The advantages of such an approach lie in the potential of such solutions to bring about further physical understanding with consequent new analytic solutions (e.g. the wake) and in the area of computer-aided-design of aircraft where the engineer requires the physical understanding. In addition, there is the advantage of reduced computer time and storage although this may be offset somewhat with the advent of larger and faster computers.

The results support the use of the unsteady cross flow analogy for three dimensional steady separated flows. A theoretically derived equivalence between two dimensional unsteady and three dimensional steady flow has been replaced by one empirical factor, σ, with physical bounds, i.e. $0 < \sigma \leq 1$ (cf. the eddy viscosity in turbulent flow). Further testing of the technique, with the use of equation (58) for σ, should shed further light on the role played by this factor.

REFERENCES

1. Hess, J. L. & Smith, A. M. O.: Calculation of Potential Flow About Arbitrary Bodies. Progr. Aero. Sci., Vol. 8, Pergamon, 1967.

2. Woodward, F.: Analysis and Design of Wing-Body Combinations at Subsonic and Supersonic Speeds. J. Aircraft, Vol. 5, No. 6, Nov.-Dec., 1968, pp. 528-534.

3. Holt, A., (edit.): Proceedings of 2nd International Conference on Numerical Methods in Fluid Dynamics. Springer-Verlag, 1971.

4. Proceedings: AIAA Computational Fluid Dynamics Conference. Palm Springs, Calif., July 19-20, 1973.

5. Thompson, J. F., Jr., Shanks, S. P. and Wu, J. C.: Numerical Solutions of Three Dimensional Navier-Stokes Equations in Integro-Differential Form Flow About a Finite Body. Ref. 4, p. 123-132.

6. Tinling, B. E. and Allen, C. Q.: An Investigation of the Normal Force and Vortex Wake Characteristics of an Ogive-Cylinder Body at Subsonic Speeds. NACA TN D-1297, 1962.

7. Jones, R.: Distribution of Normal Pressures on Prolate Spheroid. R&M 1061, Brit. A. R. C., 1925.

8. Morrison, A. M., and Ingram, C. W.: Experimental Investigation of Lee Side Flow from Cone-Cylinder Model. AIAA, Vol. 9, No. 7, July 1971, pp. 1421-1423.

9. Rodgers, E. J.: Vorticity Generation of Body of Revolution at $\alpha > 0$. J. Basic Eng., Vol. 86, Dec. 1964, pp. 845-850.

10. Peake, D. J., Rainbird, W. J., and Atraghji, E. G.: Three Dimensional Flow Separation on Aircraft and Missiles. AIAA, Vol. 10, No. 5, May 1972, pp. 567-580.

11. Allen, H. J. and Perkins, E. W.: A Study of Effects of Viscosity on Flow Over Slender Inclined Body of Revolution. NASA Rept. 1048, 1951.

12. Jorgensen, L. H. and Perkins, E. W.: Investigation of Some Wake Vortex Characteristics of an Inclined Ogive-Cylinder Body at $M = 2$. NASA Rept. 1371, 1958.

13. Thwaites, B. (edit): Incompressible Aerodynamics. Oxford, 1960, 409ff.

14. Bryson, A. E.: Symmetric Vortex Separation on Circular Cylinders and Cones. J. Appl. Mech., Vol. 26, Dec. 1959, pp. 643-648.

15. Sarpkaya, T.: An Analytical Study of Separated Flow About Circular Cylinder. J. Basic Eng., Vol. 90, Dec. 1968, pp. 511-520.

16. Marshall, F. J.: Impulsive Motion of a Cylinder and Viscous Cross Flow. J. Aircraft, Vol. 7, No. 4, July-Aug. 1970, pp. 371-373.

17. Walitt, L., Trulio, J. G., and King, L. S.: A Numerical Method of Computing Three-Dimensional Viscous Supersonic Flow Fields About Slender Bodies. NASA SP-288, 1969, pp. 265-322.

18. Schindel, L.: Effects of Vortex Separation on Lift Distribution of Elliptic Cross Section. J. Aircraft, Vol. 6, No. 6, Nov.-Dec. 1969, pp. 537-543.

19. Kelly, H.: Estimate of Normal Force and Pitching Moment for Blunt Based Body of Revolution. JAS., Vol. 21, No. 8, August 1954, pp. 549-555, 565.

20. Lavender, R. E.: Application of Kelly's Theory to Cone-Cylinder-Frustrum Body of Revolution. JAS., Vol. 22, No. 9, Sept. 1955, pp. 654-655.

21. Mello, J. F.: Investigation of Normal Force Distribution and Wake Vortex Characteristics of Body of Revolution M > 1. JAS., Vol. 26, No. 3, Mar. 1959, pp. 155-168.

22. Jorgensen, L. H.: Estimation of Aerodynamics for Slender Bodies Alone and With Lifting Surfaces at α = 0 to 90°. AIAA, Vol. 11, No. 3, Mar. 1973, pp. 409-412.

23. Thompson, K. D., and Morrison, D. F.: The Spacing Position and Strength of Vortices in the Wake of Slender Cylindrical Bodies at Large Incidence. Aus. Def. Sci. Serv., Report HSA 25, June 1969.

24. Kuchemann, D. and Weber, J.: Vortex Motions. ZAMM, Vol. 45, Dec. 1965, pp. 457-474.

25. Wang, K. C.: Zones of Influence and Dependence for Three Dimensional Boundary Layer Equations. J. Fluid Mech., Vol. 48, Part 2, 28 July 1971, pp. 397-404.

26. Kuchemann, D. (edit.): Progr. Aero. Sci., Vol. 7, Pergamon 1966.

27. Hackett, J. E. and Evans, M. R.: Vortex Wakes Behind High Lift Wings. J. Aircraft, Vol. 8, No. 5, May 1971, pp. 334-340.

28. Yang, H. T.: A Vortex Method for the Study of Airplane and Missile Aerodynamic Interference. J. Aircraft, Vol. 5, No. 6, Nov.-Dec. 1968, pp. 591-597.

29. Finkleman, D.: Non-linear Vortex Interaction on Wing-Conard Configuration. J. Aircraft, Vol. 9, No. 6, June 1972, pp. 399-406.

30. Sacks, A. H., Lundberg, R. E., and Hanson, C. W.: Theoretical Investigation of Aerodynamics of Slender Wing-Body Combinations Exhibiting Leading Edge Separation. NASA CR-719, March 1967.

31. Hill, J. A. F.: Nonlinear Theory of Lift of Slender Bodies of Revolution. Navord Report 5338, October 1954.

32. Wundt, H.: Wach stum der laminaren Grenzschicht an schräg ange stromten Zylinder bei Anfahrt ans der Ruhe; Ingen-Arch, Vol. 23, 1955, pp. 212-230.

33. Morkovin, M.: Flow Around Circular Cylinder - a Kaleidoscope of Challenging Fluid Phenomena. ASME Symposium on Fully Separated Flows, Phil., Pa., May 1964.

34. Thoman, D. C. and Szewiczyk, A. A.: Time Dependent Viscous Flow Viscous Flow Over a Circular Cylinder. Phys. Fluids, Suppl. II, 1969, pp. II-76 - II80.

35. Hall, M. G.: A Numerical Method for Calculating the Unsteady Two Dimensional Laminar Boundary Layer. Ing-Arch, Vol. 38, 1969, pp. 97-106.

36. Marshall, F. J. (edit.): Fluid Dynamics of Unsteady, Three Dimensional and Separated Flows. Proceedings of Project Squid Workshop, June 10-11, 1971. (Available from Project Squid Headquarters, Purdue University).

37. Sears, W. R. and Telionis, D. P.: Unsteady Boundary Layer Separation. IUTAM Symposium, 1971, pp. 404-447.

38. Telionis, D. P. and Tshalis, D. Th.: The Response of Unsteady Boundary Layer Separation to Time Dependent Outer Flows. Paper 73-684, AIAA, 1973.

39. Schaefer, J. W. and Eskinazi, S.: The Vortex Street Generated in a Viscous Fluid. J. Fl. Mech., Vol. 6, Part 2, Aug. 1959, pp. 241-260.

40. Taneda, S.: Visualization Experiments on Unsteady Flows Around Cylinders and Plates. IUTAM Symposium, 1971, pp. 1165-1215.

41. Pierce, D.: Photographic Evidence of the Formation and Growth of Vorticity Behind Flat Plate Accelerated from Rest in Still Air. J. Fl. Mech., Vol. 11, Part 3, Nov. 1961, pp. 460-465, 1961.

42. Abernathy, F. H., and Kronauer, R. E.: Formation of Vortex Sheets. J. Fl. Mech., Vol. 13, Part 1, May 1962, pp. 1-20, 1962.

43. Gerard, J. H.: Mechanism of Formation Region of Vortices Behind Bluff Bodies. J. Fl. Mech., Vol. 25, Part 2, June 1960, pp. 401-413.

44. Fage, H., and Johansen, F. C.: On the Flow of Air Behind an Inclined Flat Plate of Infinite Span. Proc. Roy. Soc., Series A, Vol. 116, 1927, pp. 170-197.

45. Roshko, A.: On the Drag and Shedding Frequency of Two Dimensional Bluff Bodies: NACA TN 3169, 1954.

46. Wang, K. C.: Three Dimensional Boundary Layer Near Plane of Symmetry of a Spheroid of Incidence. J. Fluid Mech., Vol. 43, Part 1, Aug. 1970, pp. 187-209.

47. Eichenbrenner, E. A. and Oudant, A.: Methode de Calcul de la Couche Limite Tridimensionelle Application a un Corps Fuselle Incline Sur le Vent. ONERA Publication No. 76, 1955.

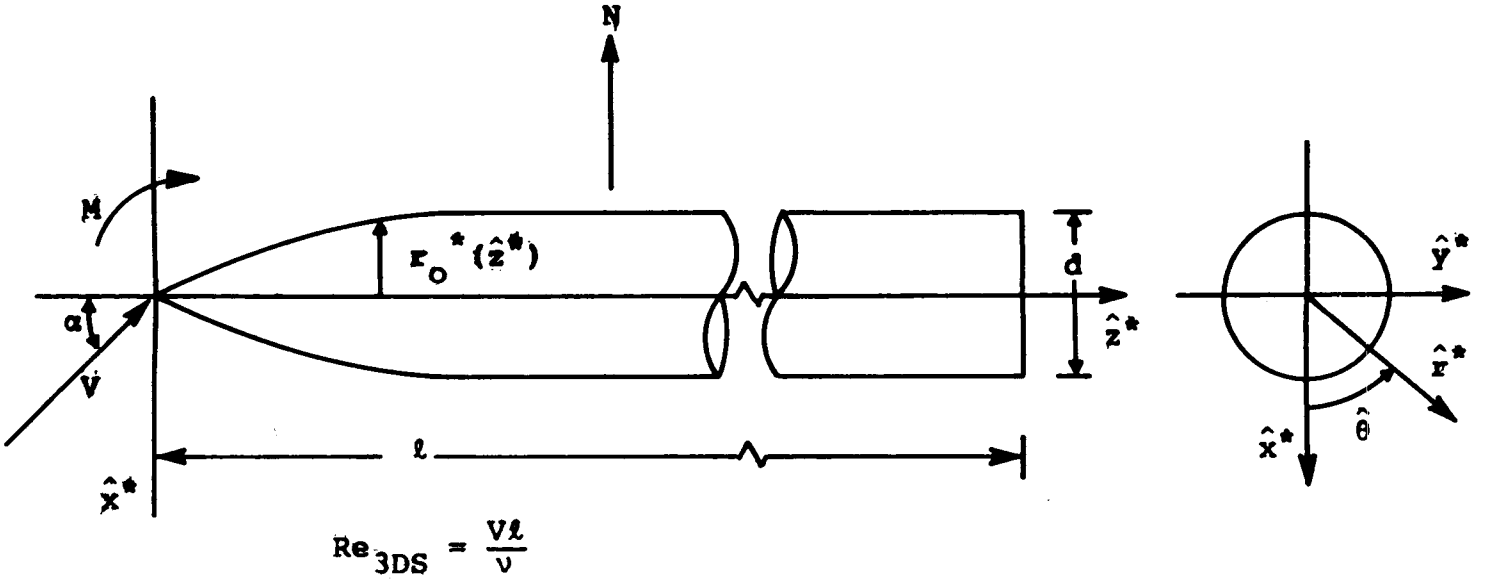

Figure 1 - Coordinate System, Body of Revolution

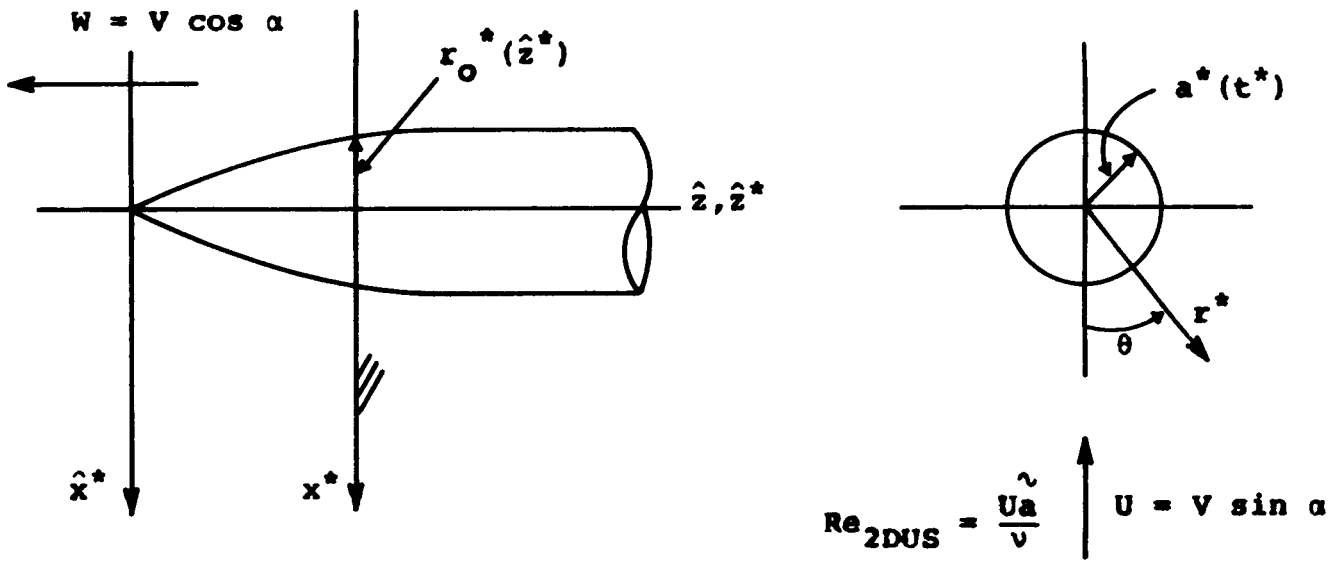

(a) - Translation

(b) - Cross Flow

Figure 2 - Coordinate Systems of Transformation, Equations (1).

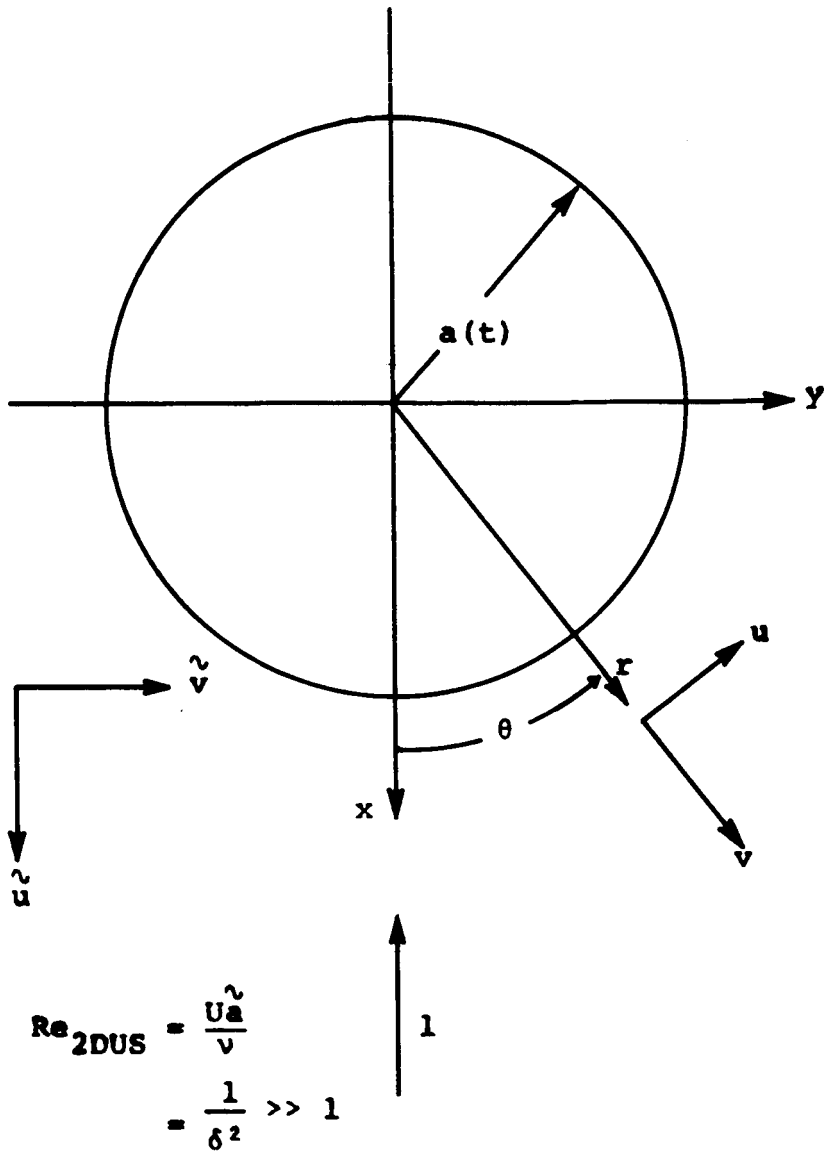

Figure 3 - Coordinate System (non-dimensional) for Unsteady Cross Flow.

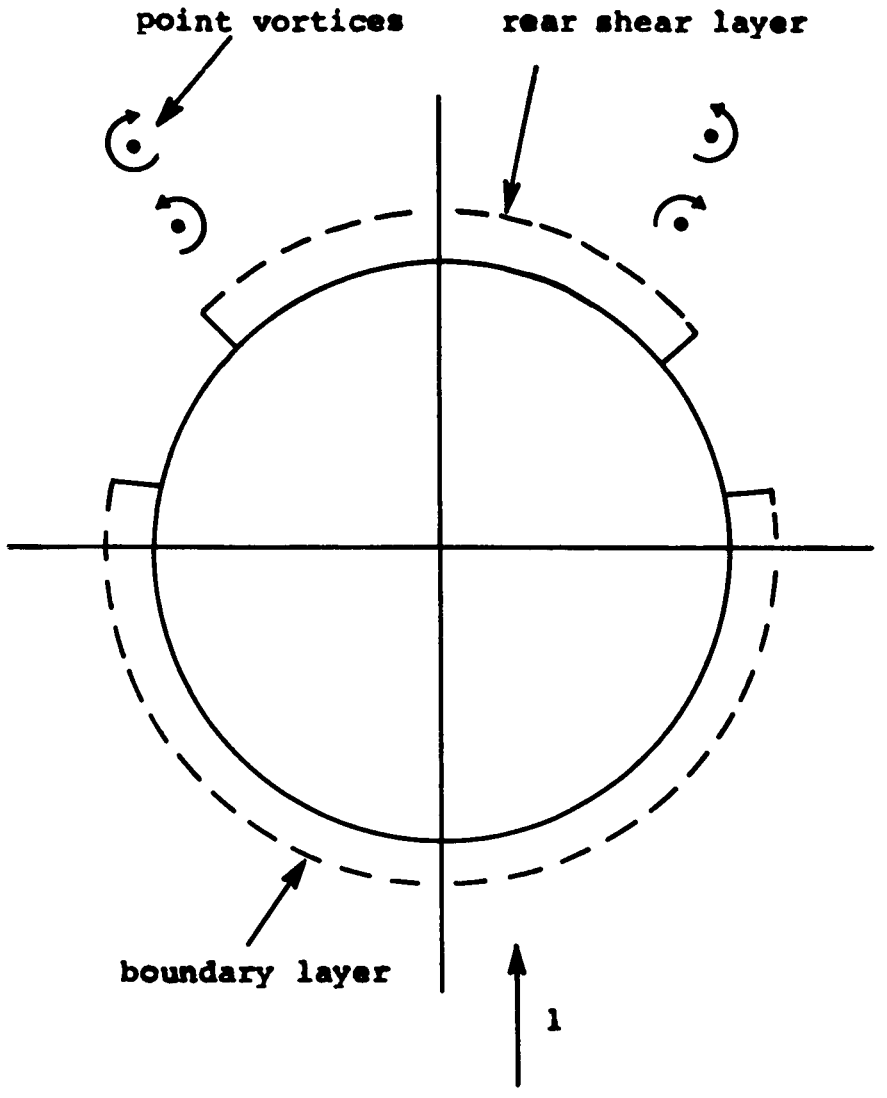

Figure 4 - Outer and Inner Flows.

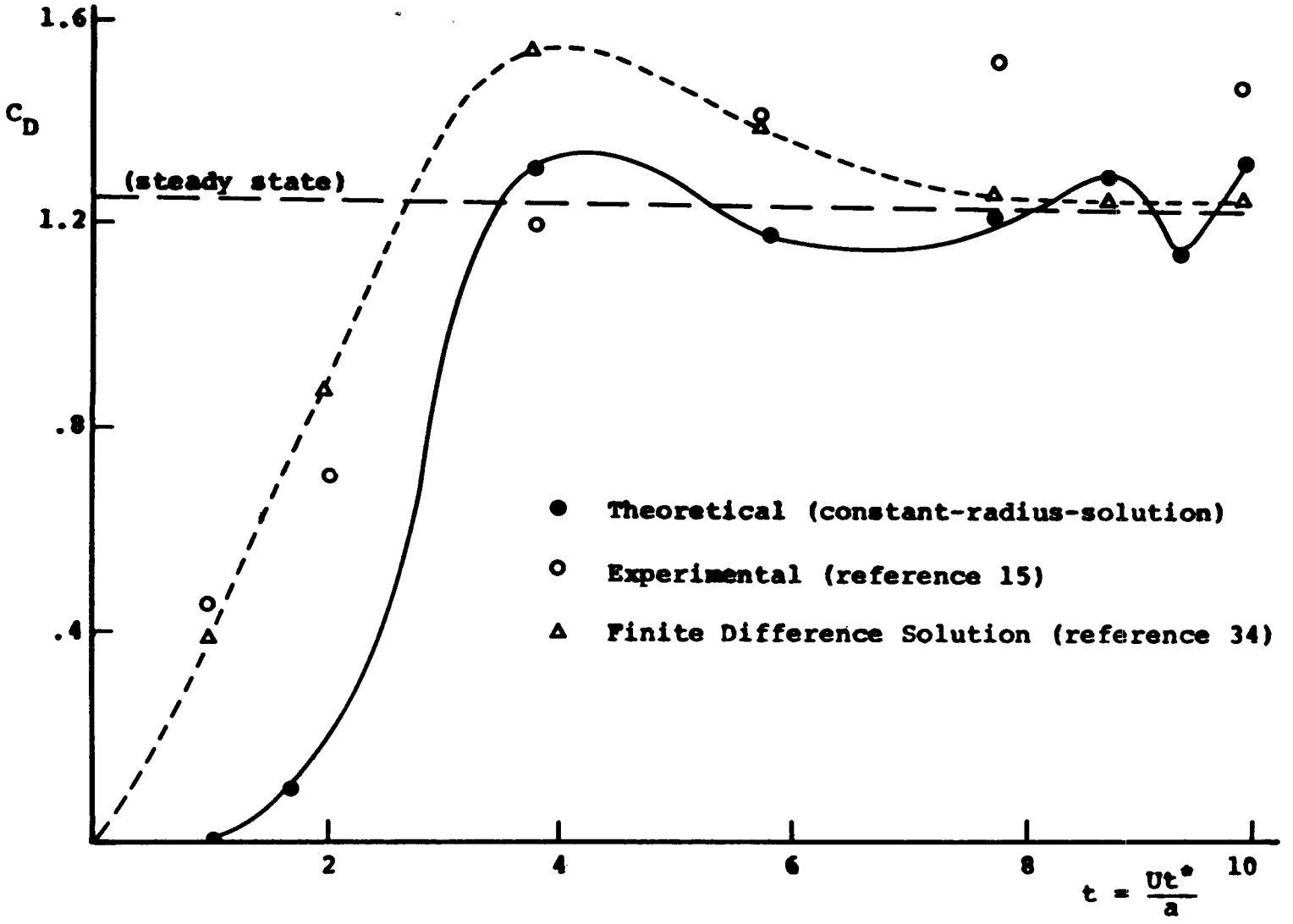

Figure 5 - Comparison of Drag Coefficients for Impulsive Flow of Cylinder of Constant Radius.

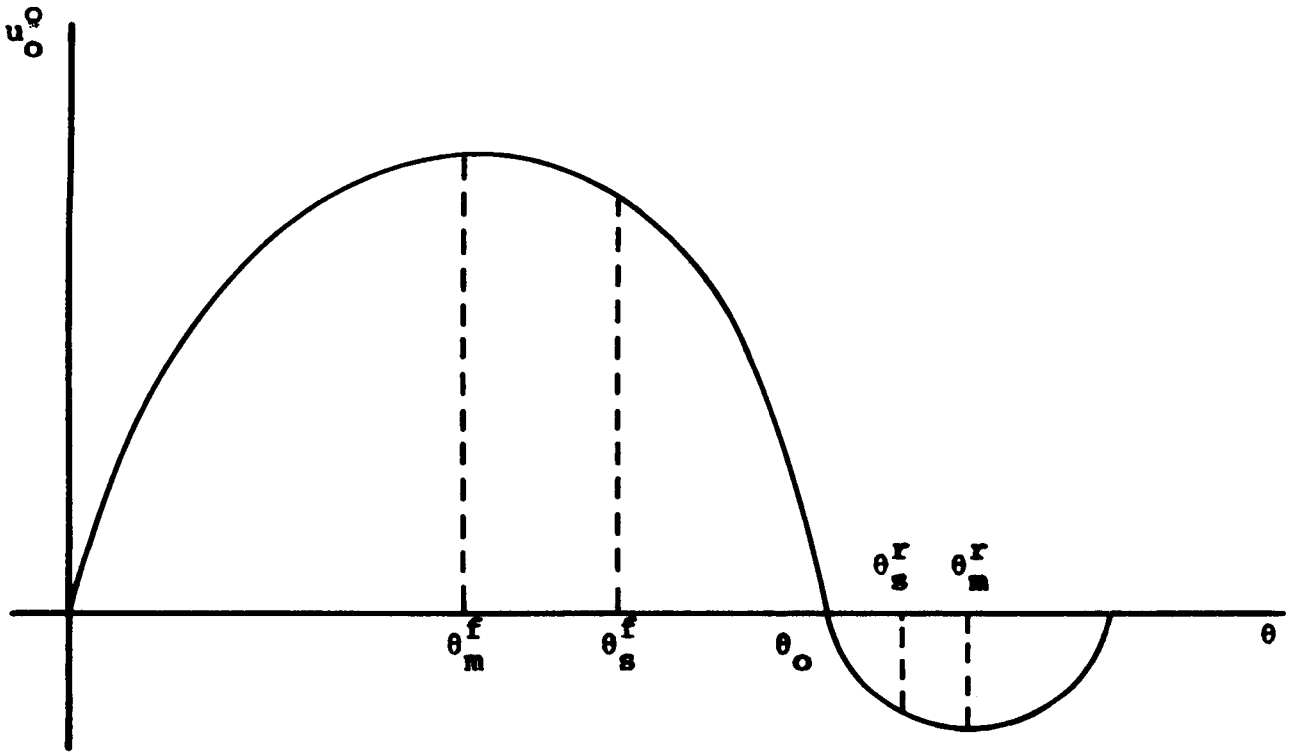

Figure 6 - Rear Shear Layer Separation Scheme.

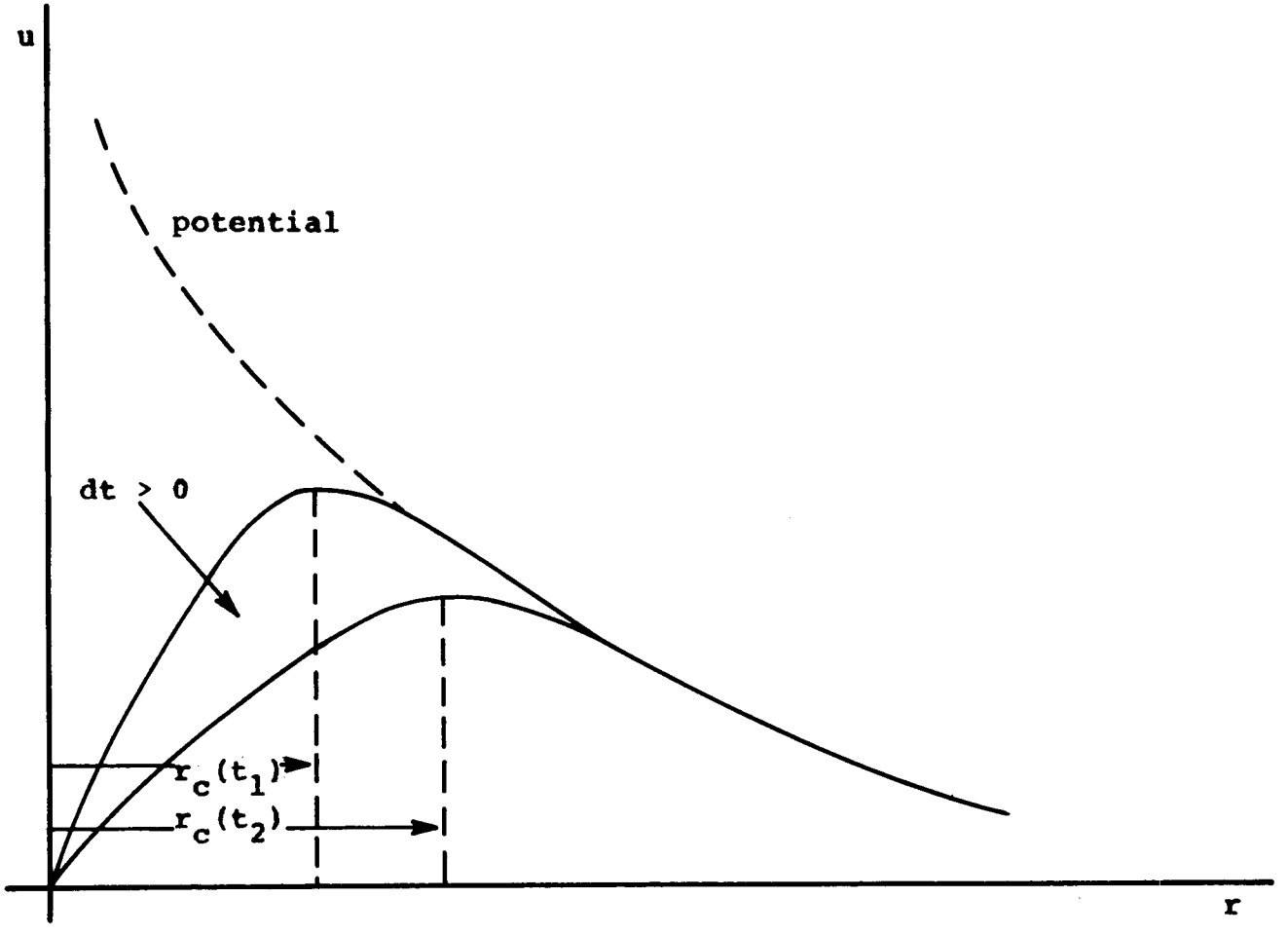

Figure 7 - Viscous Core Radius Scheme.

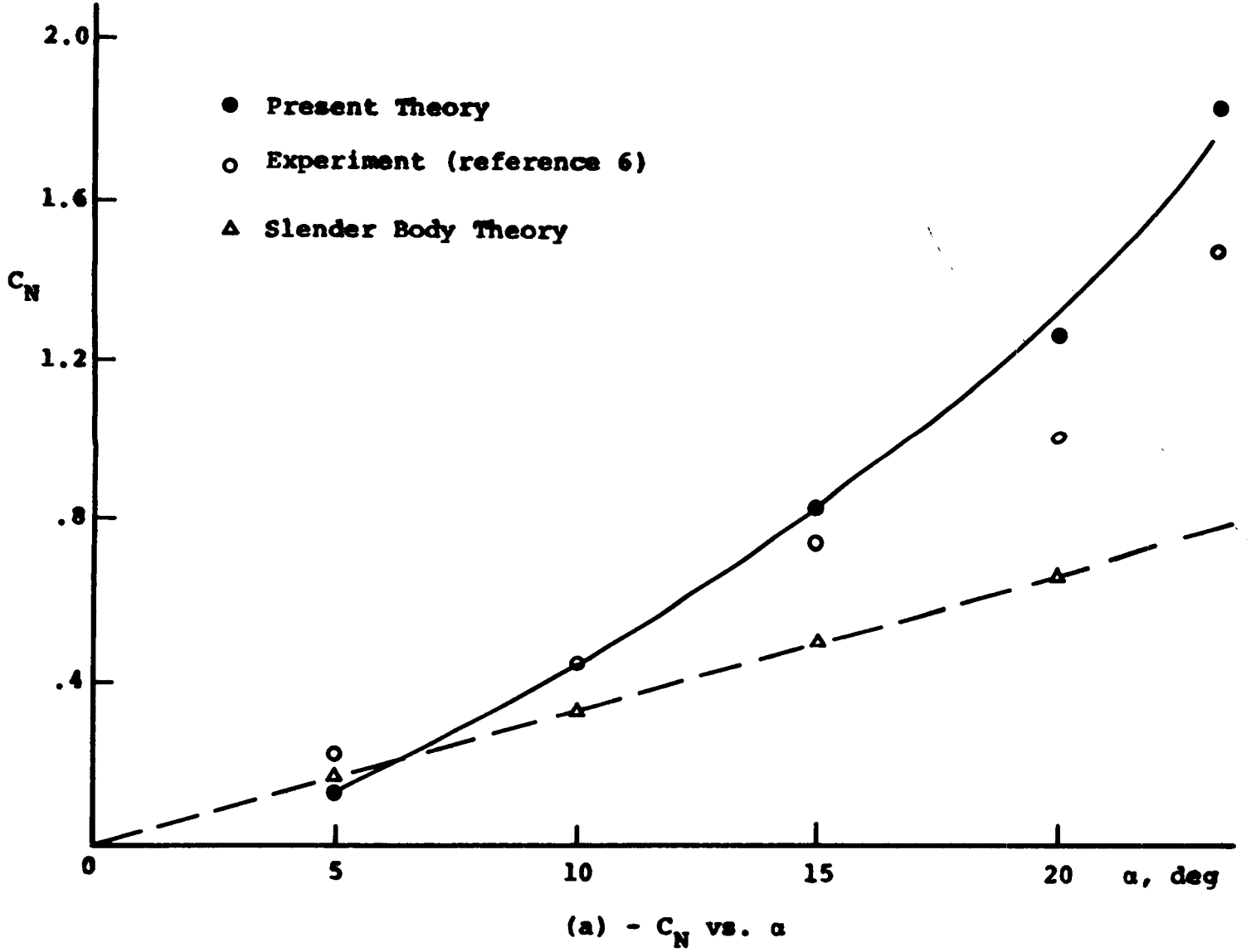

(a) - C_N vs. α

Figure 8 - Aerodynamic Characteristics of Ogive-Cylinder.

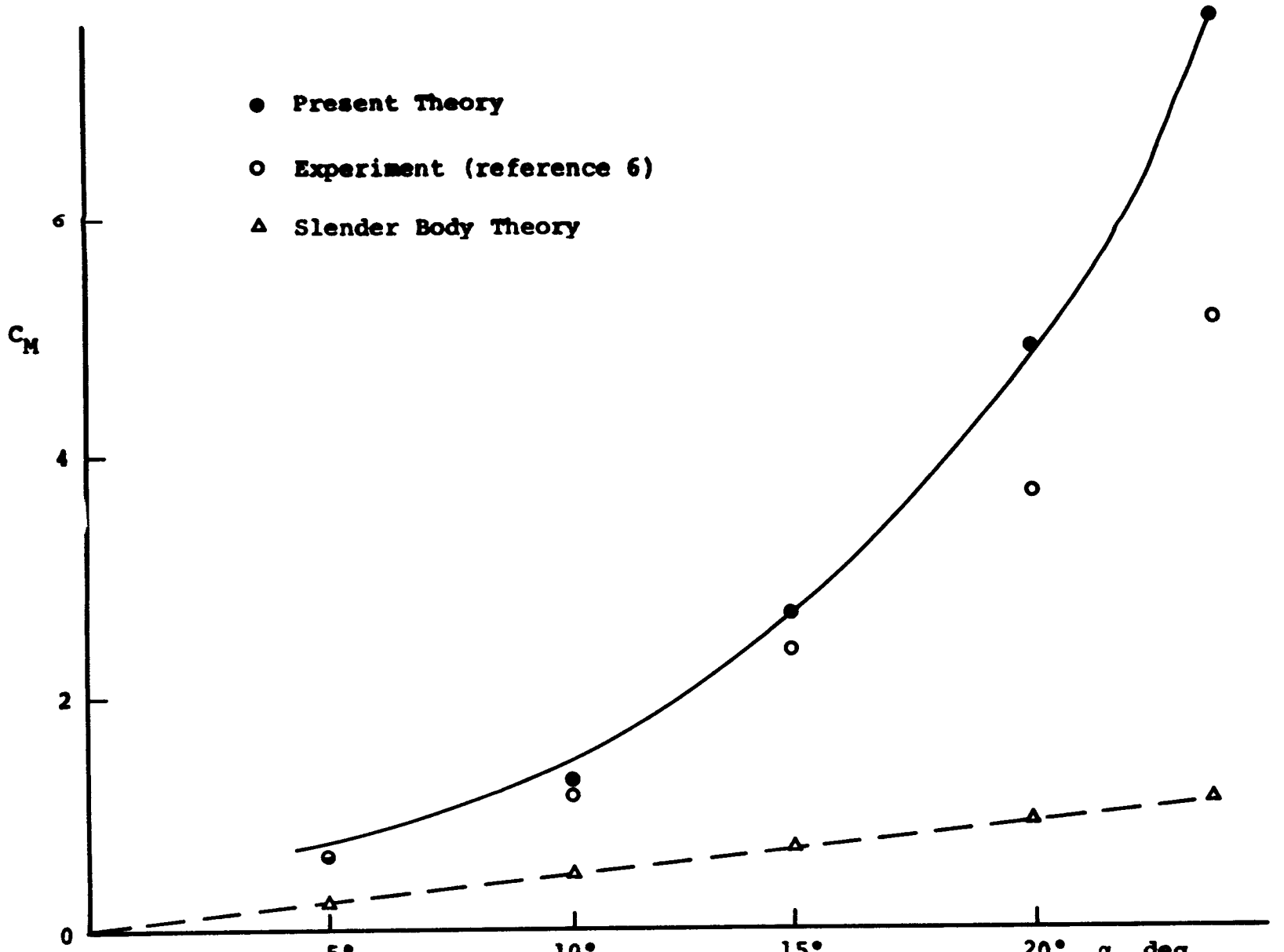

(b) - C_M vs. α

Figure 8 - Concluded

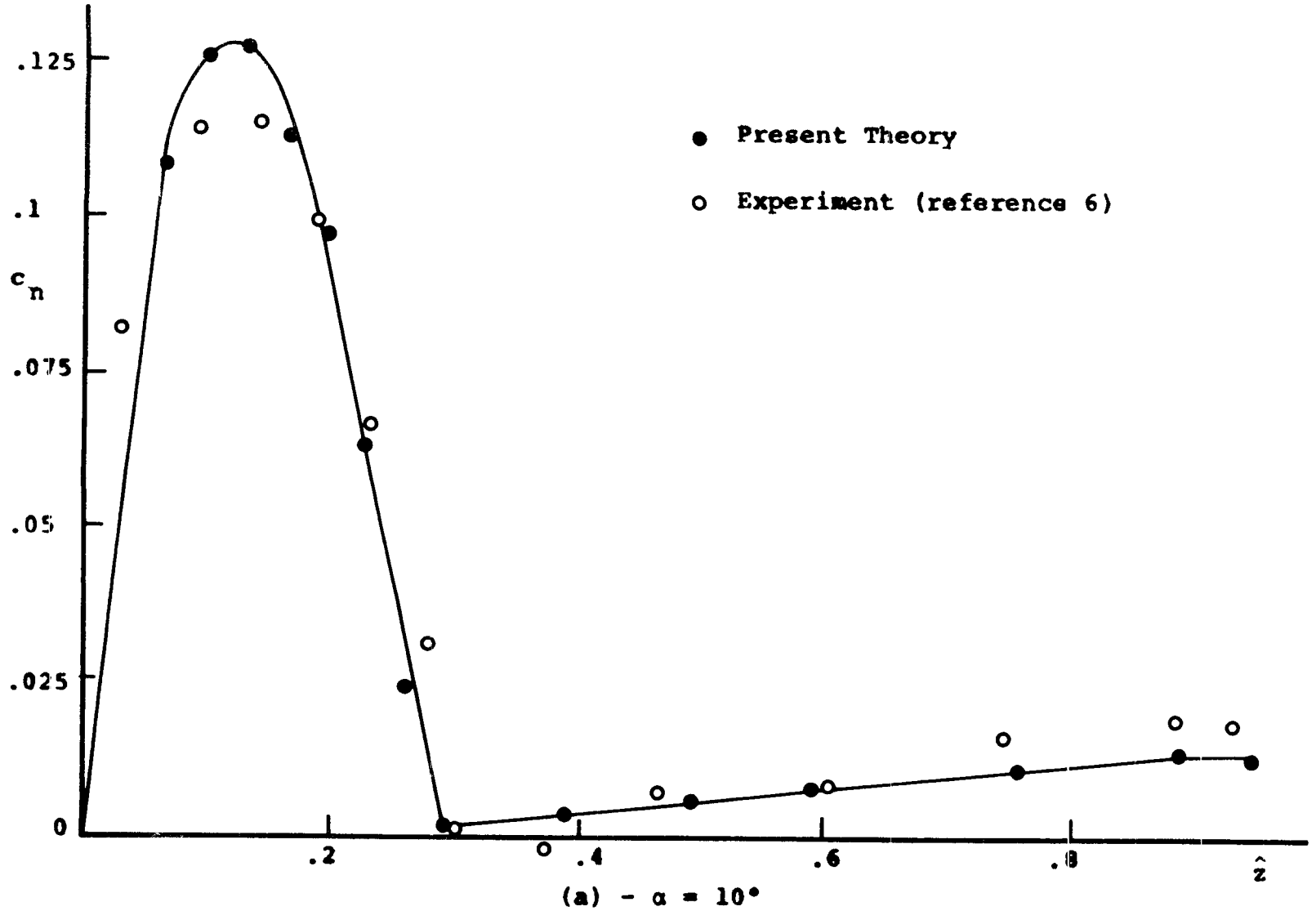

Figure 9 - Normal Force Distribution on Ogive Cylinder.

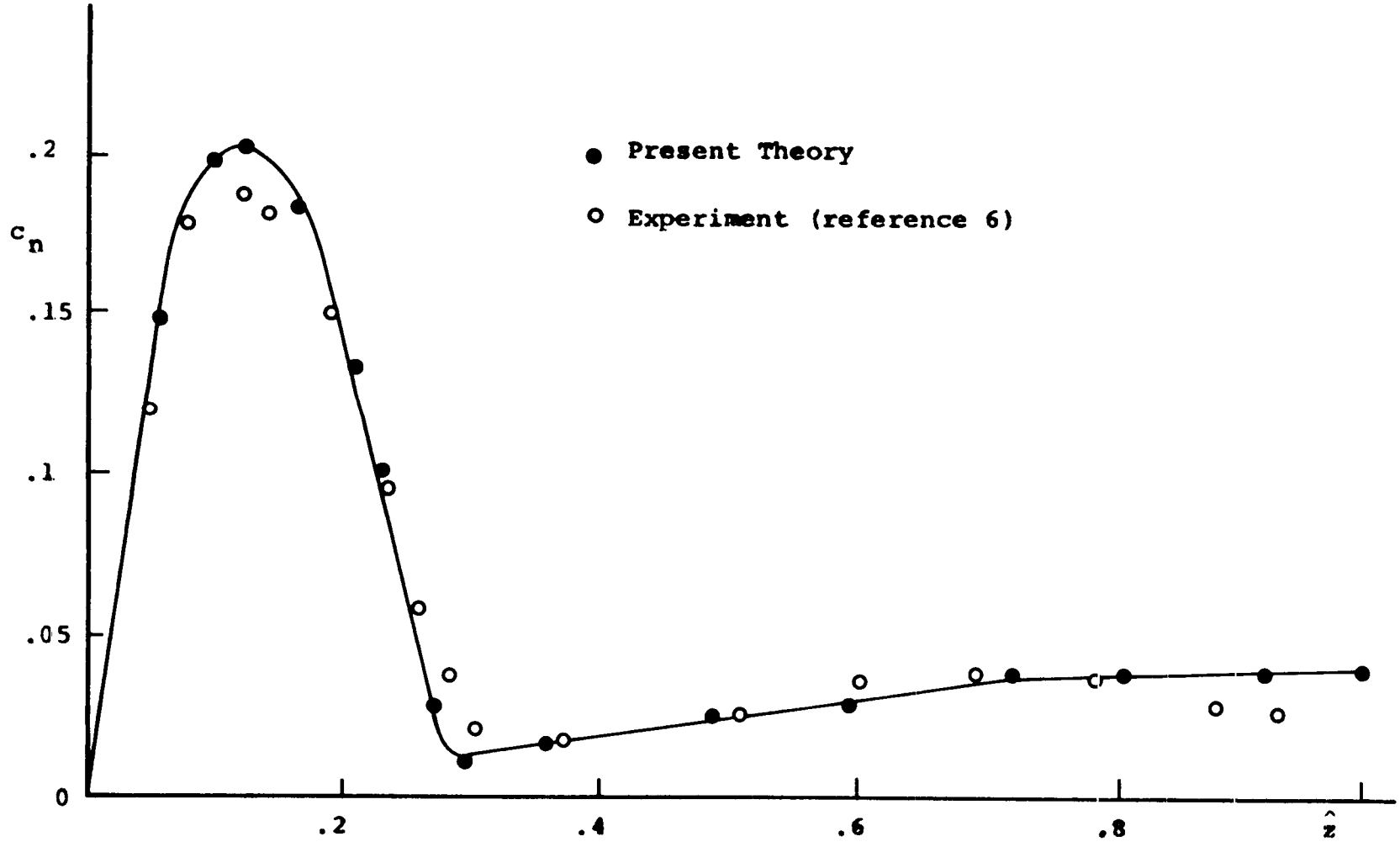

(b) - $\alpha = 15°$

Figure 9 - Continued

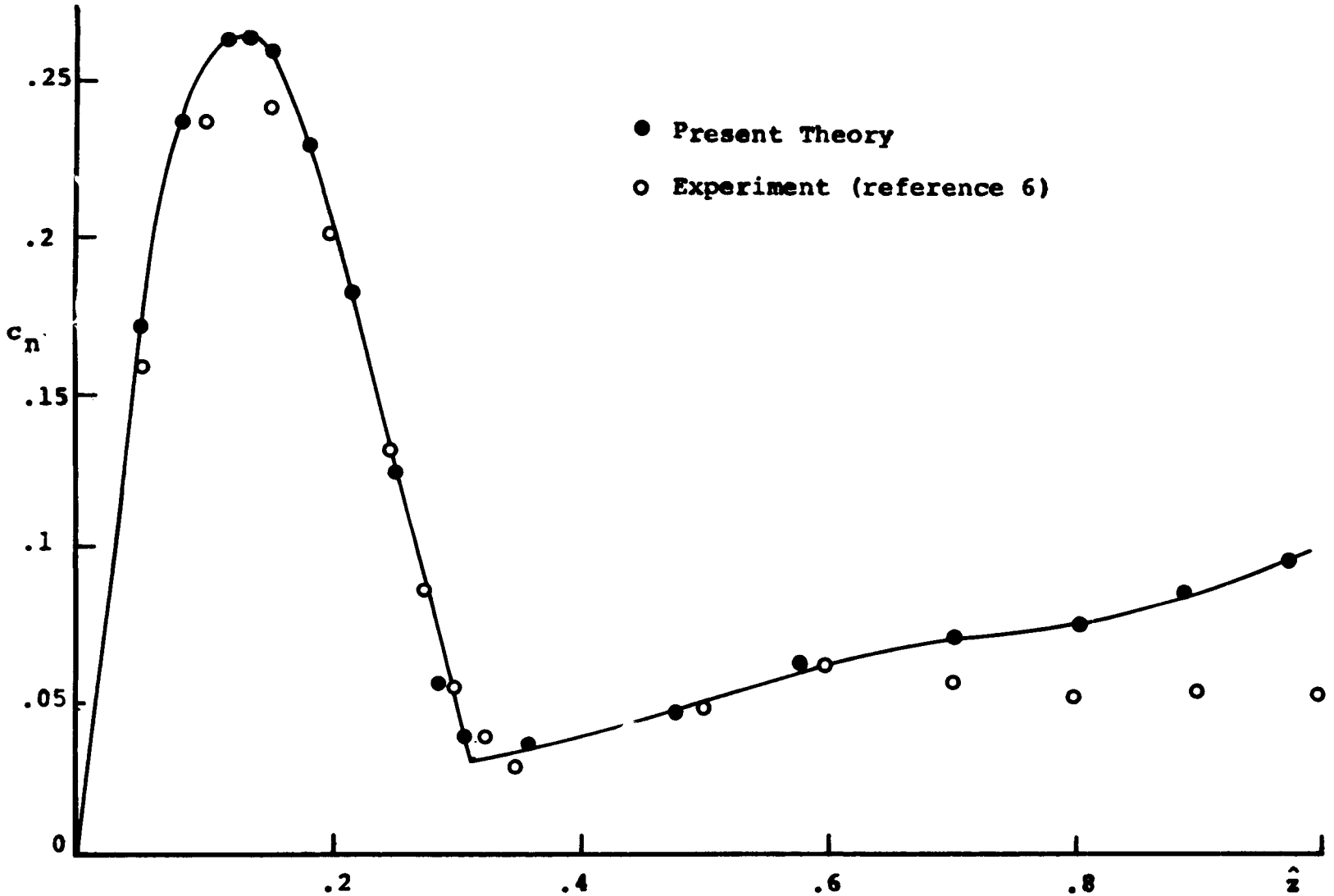

(c) - $\alpha = 20°$

Figure 9 - Continued

(d) - $\alpha = 24°$

Figure 9 - Concluded

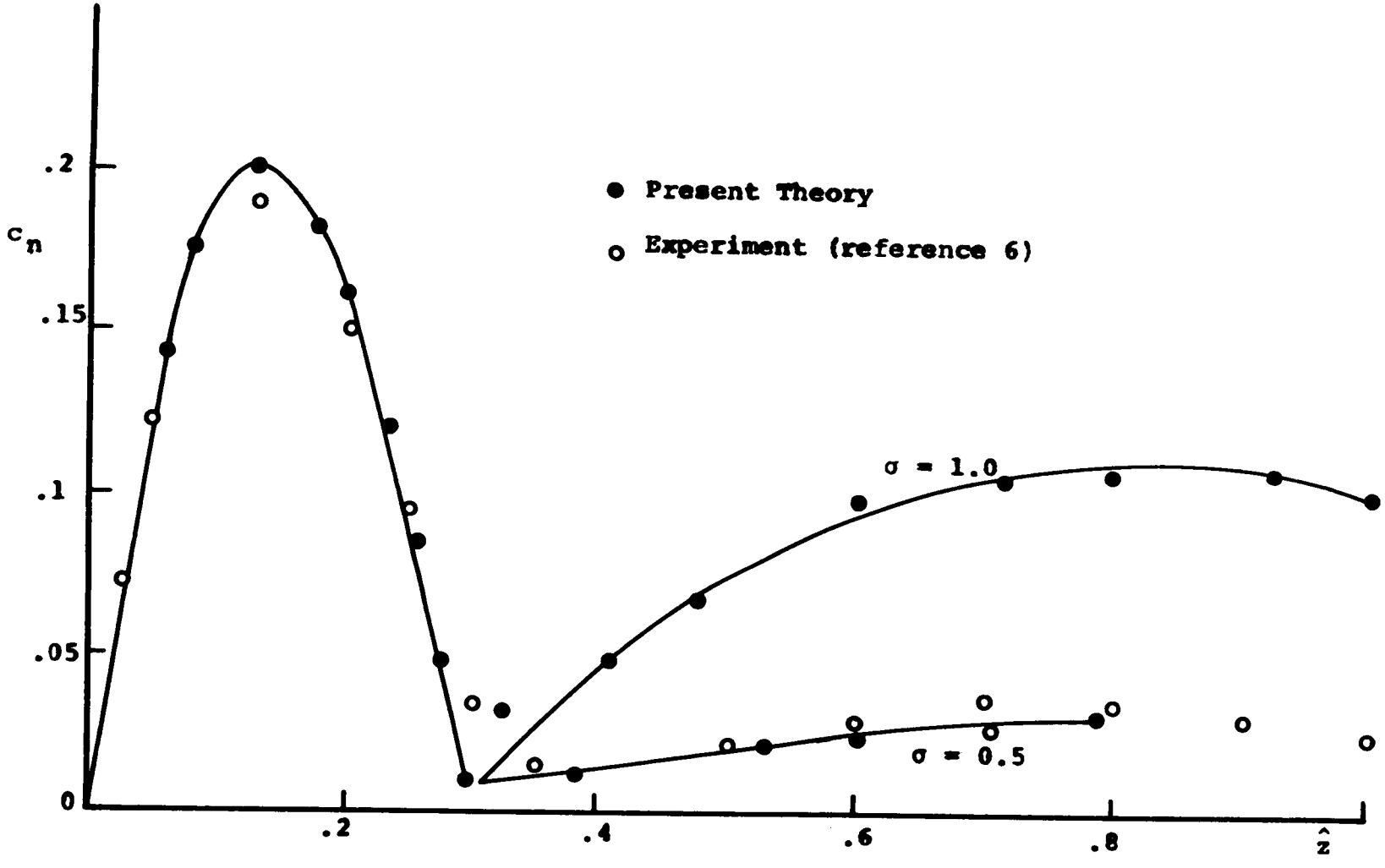

Figure 10 - Vortex Flux Effect on Normal Force Distribution, $\alpha = 15°$.

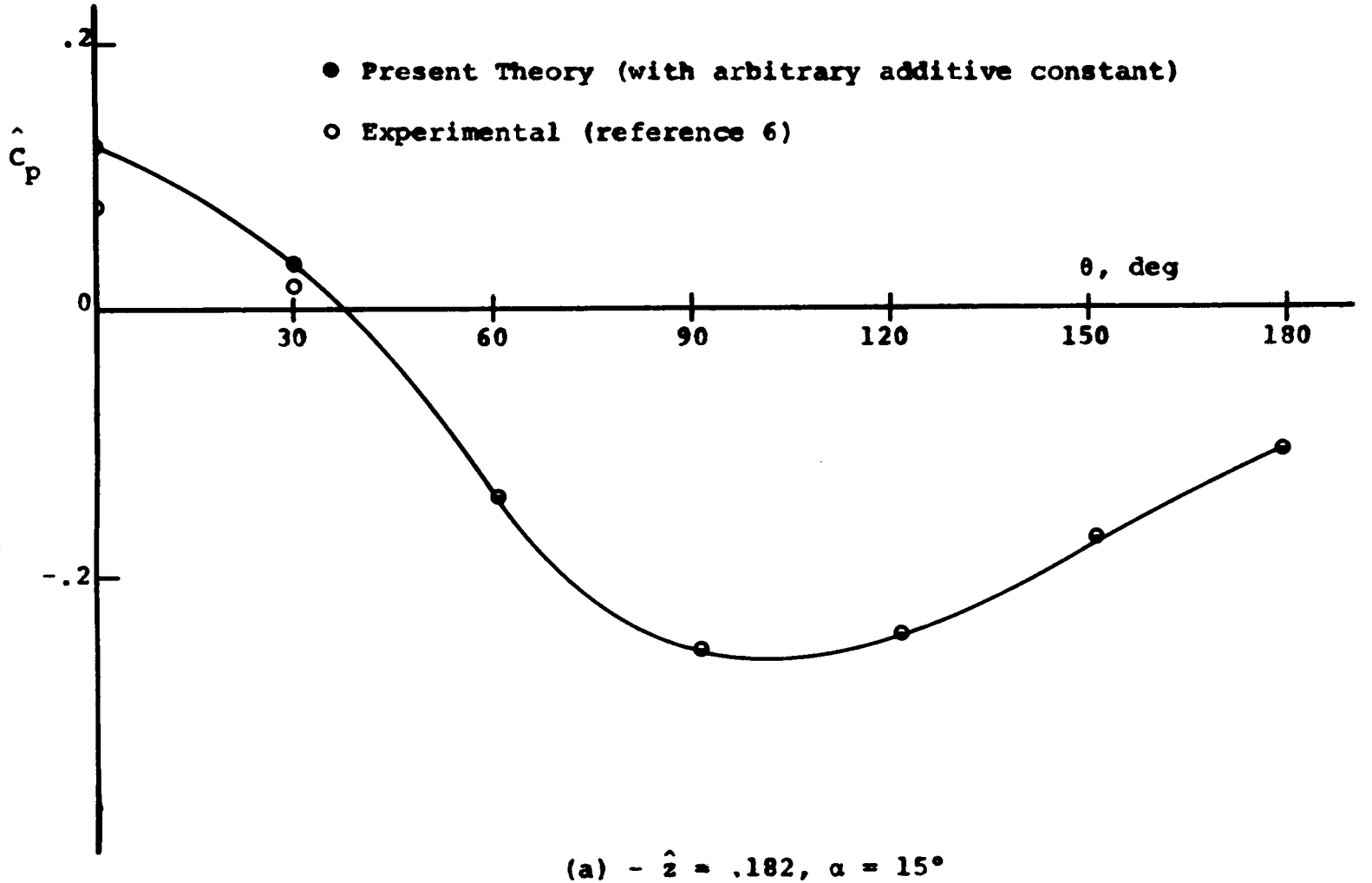

(a) - $\hat{z} = .182$, $\alpha = 15°$

Figure 11 - Pressure Distribution on Ogive-Cylinder.

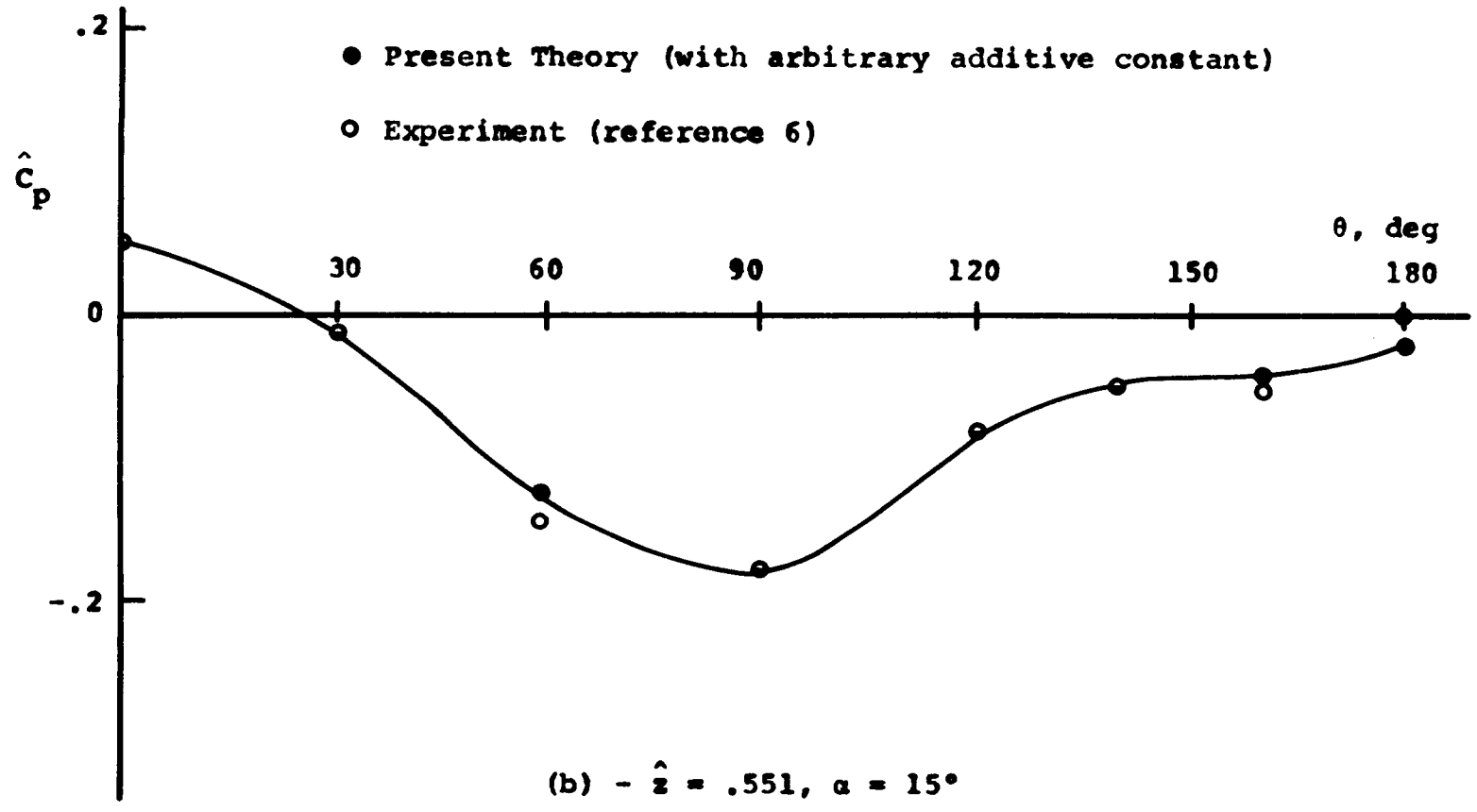

(b) - $\hat{z}$ = .551, α = 15°

Figure 11 - Continued

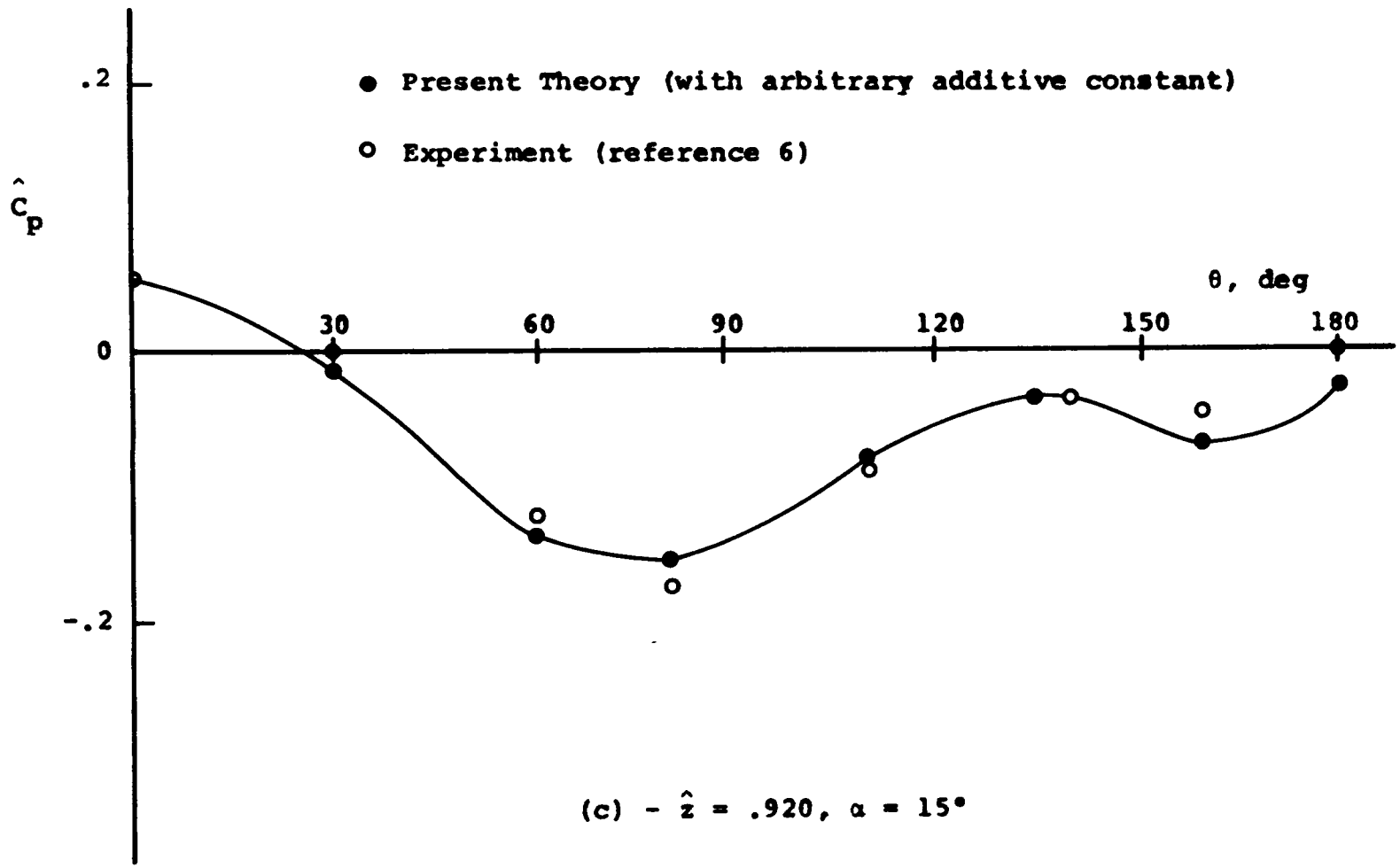

(c) - $\hat{z}$ = .920, α = 15°

Figure 11 - Continued

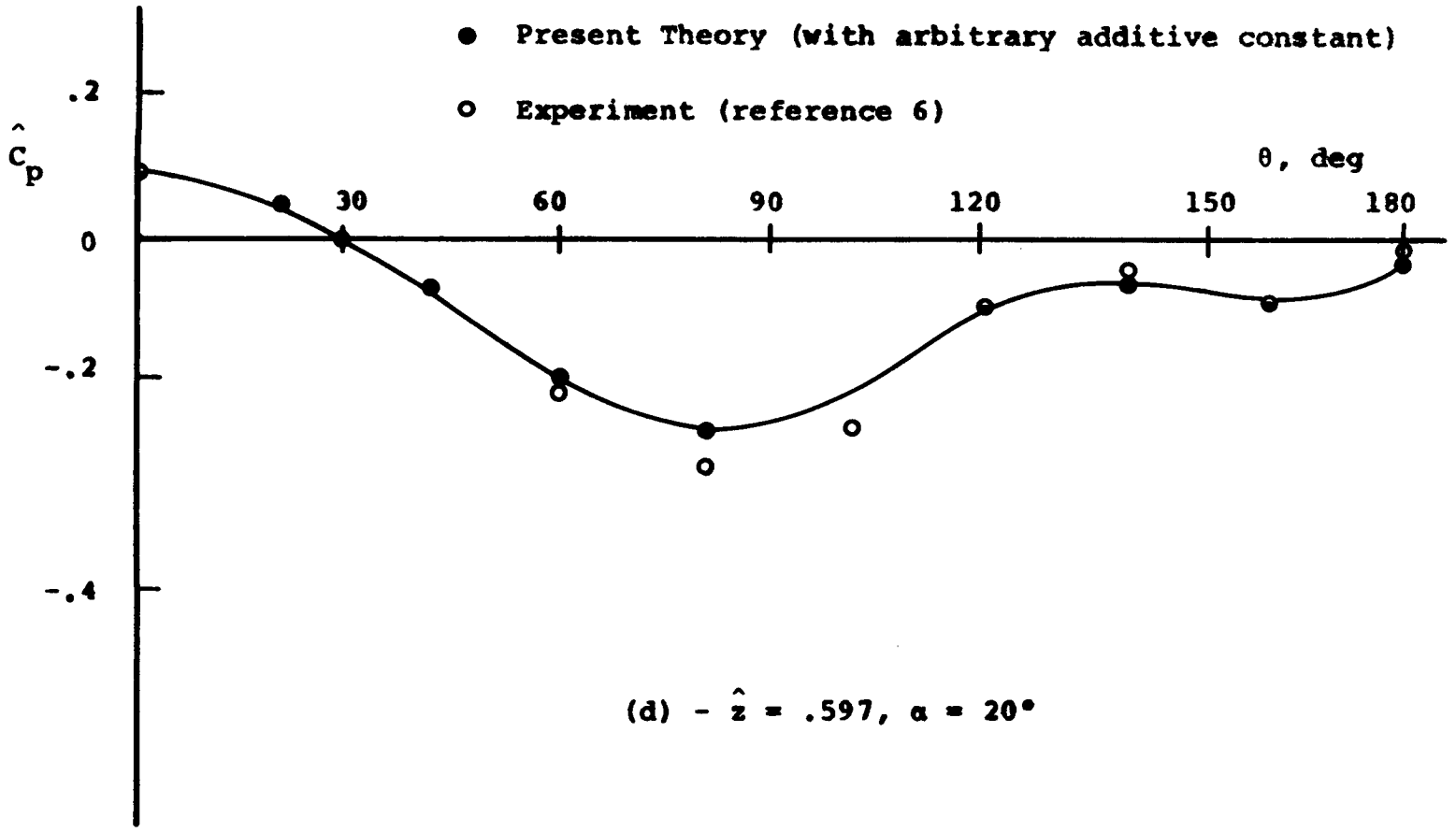

(d) - $\hat{z}$ = .597, α = 20°

Figure 11 - Continued

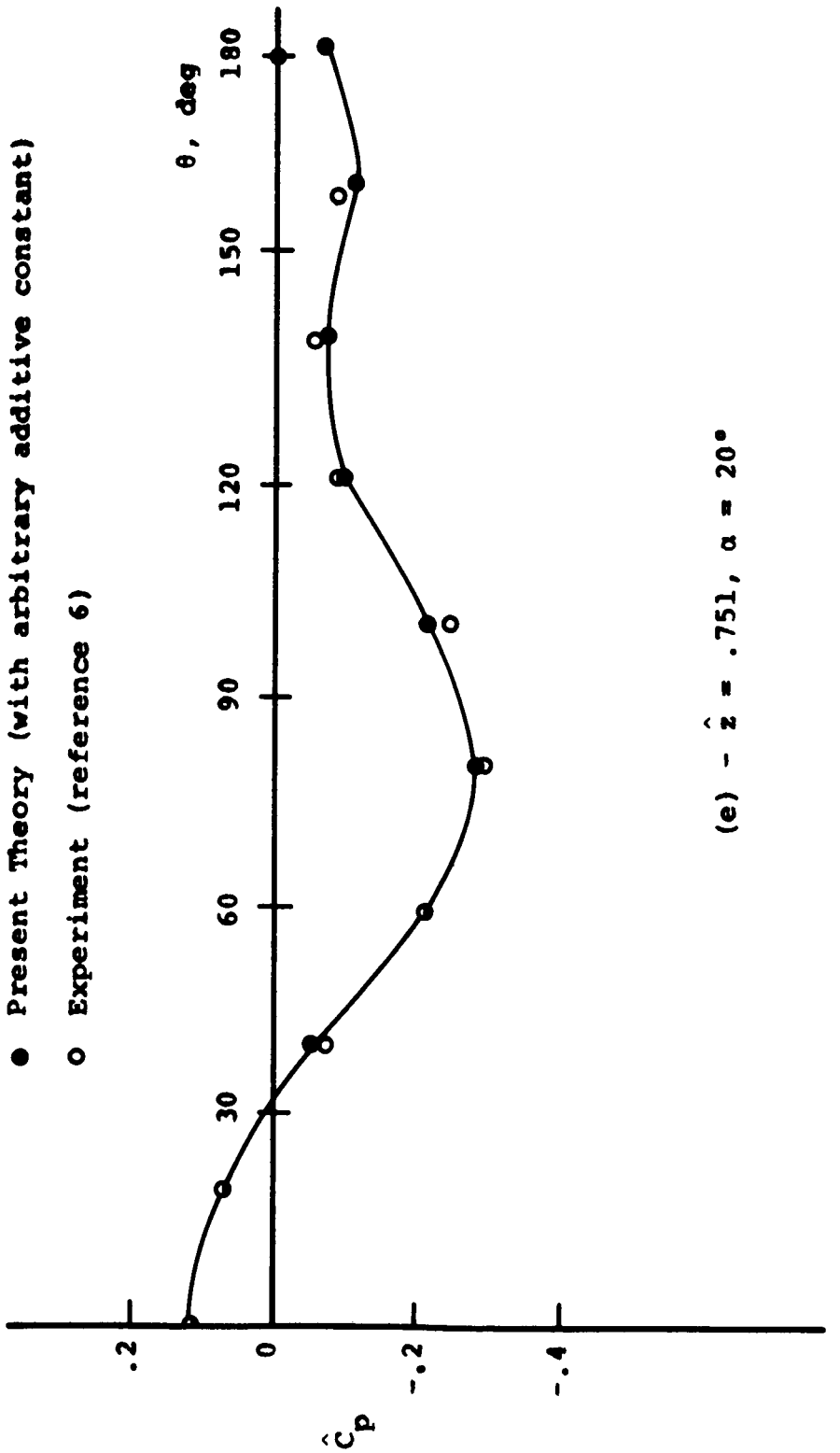

(e) - $\hat{z} = .751$, $\alpha = 20°$

Figure 11 - Continued

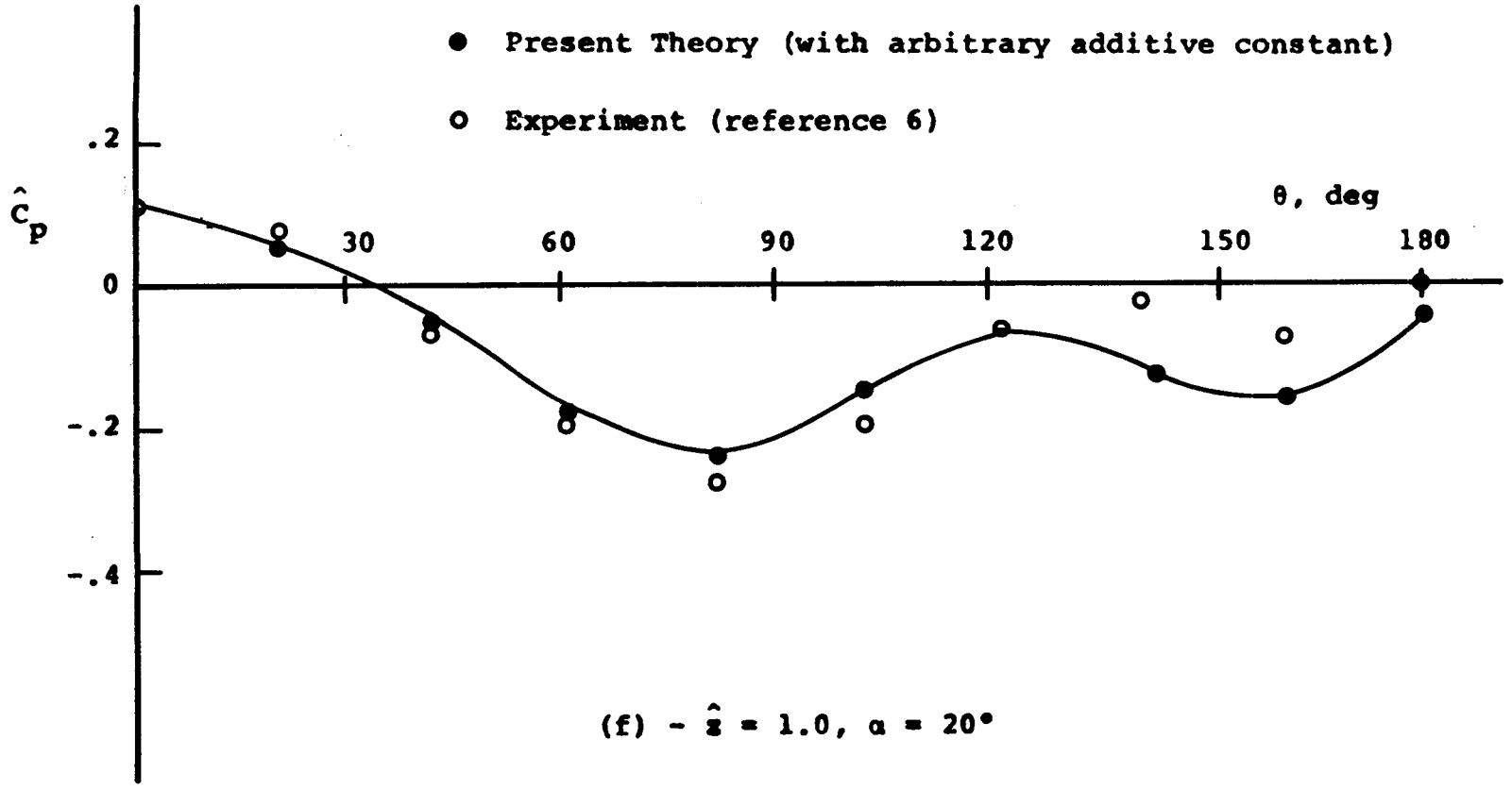

(f) - $\hat{z}$ = 1.0, α = 20°

Figure 11 - Concluded

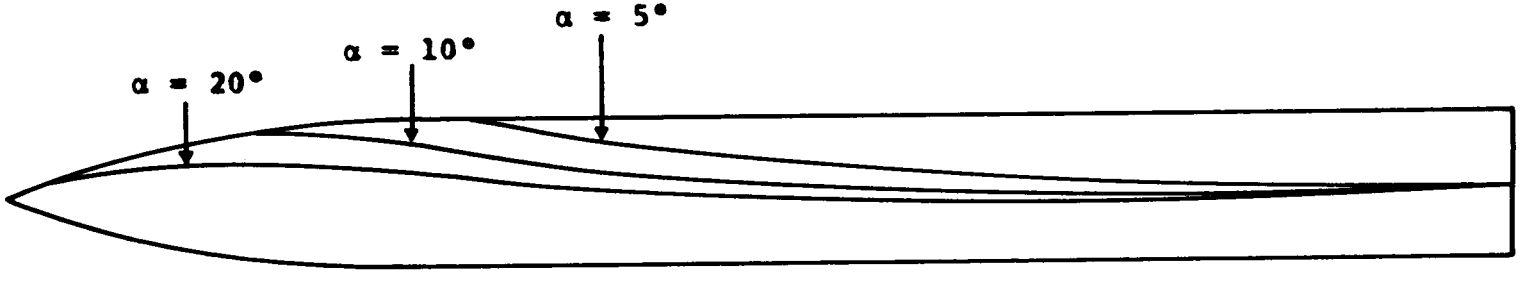

Figure 12 - Theoretical Separation Regions on Ogive-Cylinder.

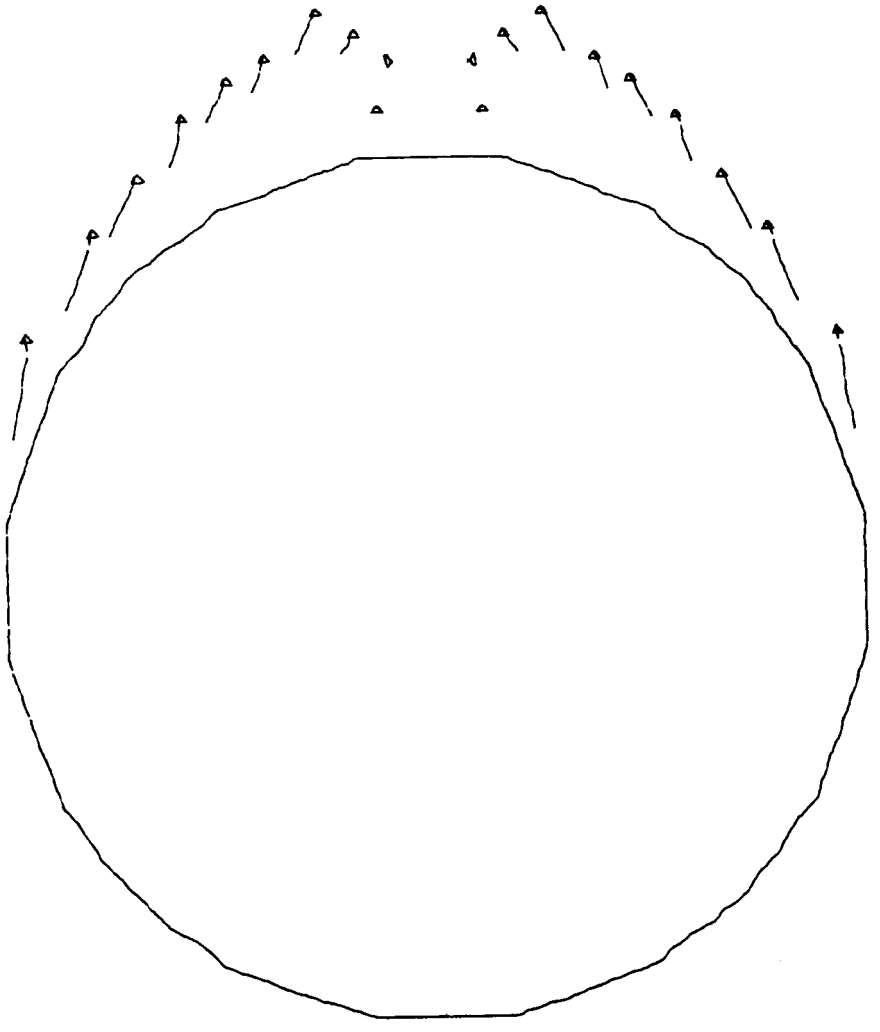

(a) - $\hat{z}$ = .202, α = 20°

Figure 13 - Wake Pattern of Ogive Cylinder.

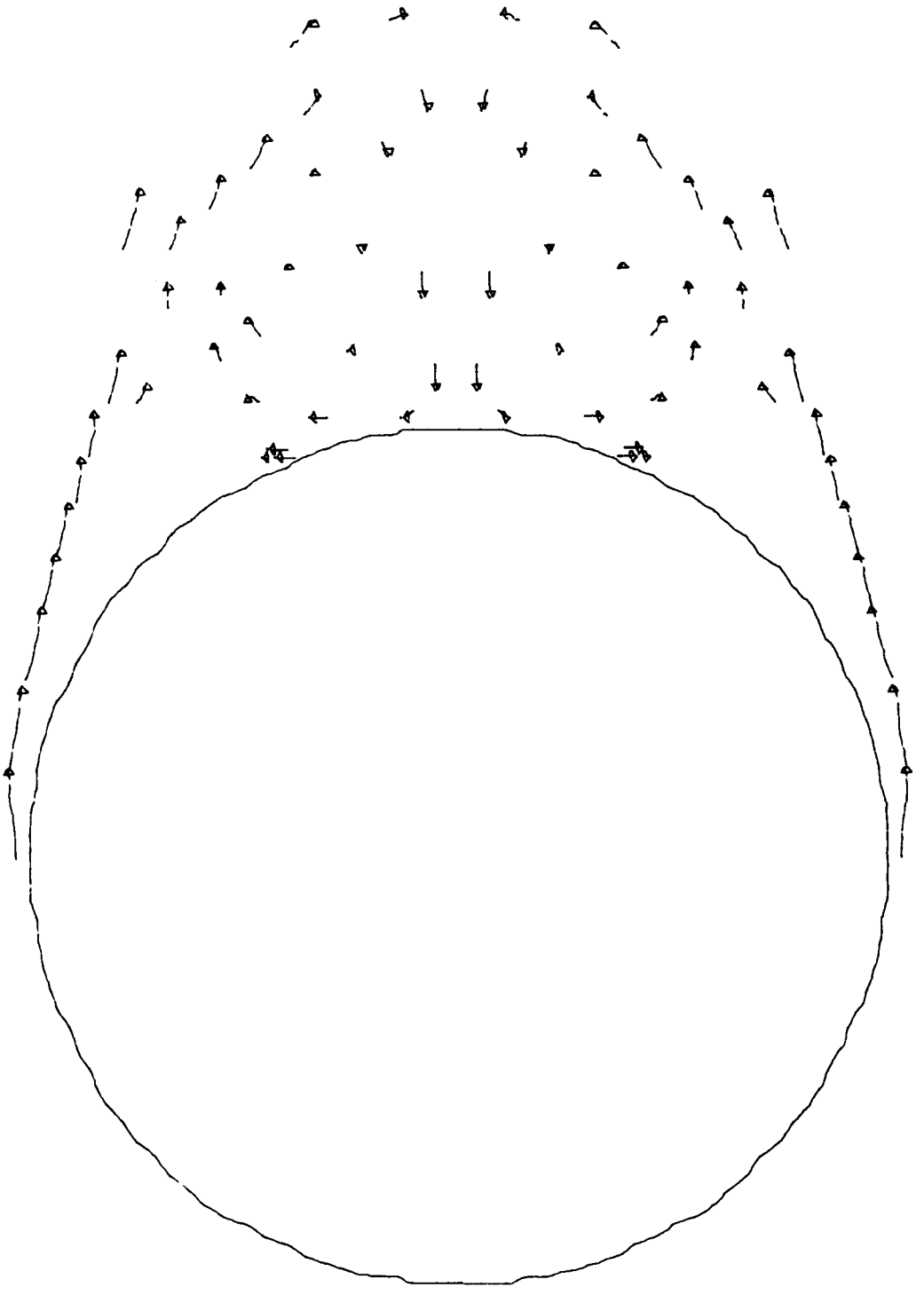

(b) - $\hat{z} = .545$, $\alpha = 20°$

Figure 13 - Continued

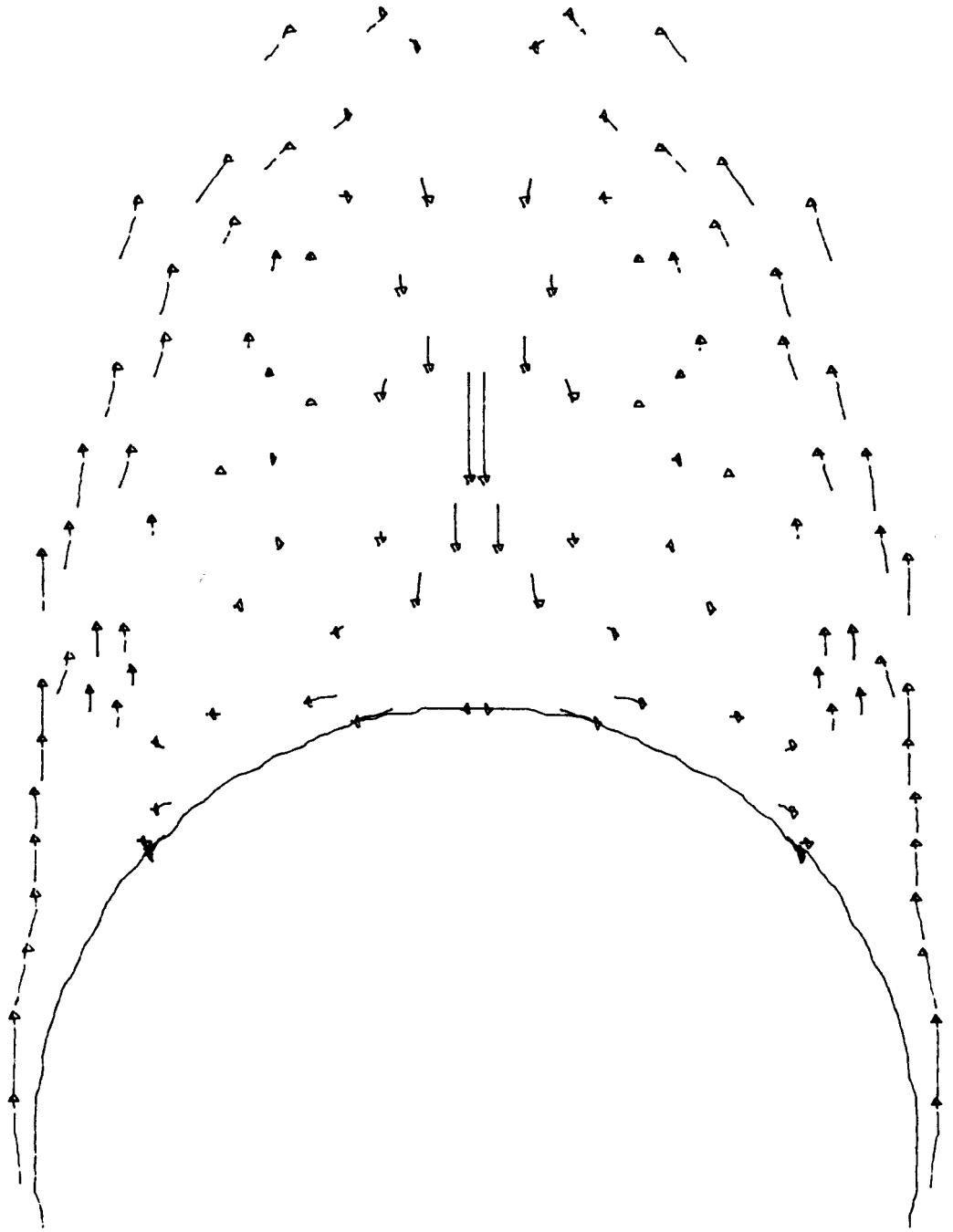

(c) - $\hat{z} = .889$, $\alpha = 20°$

Figure 13 - Concluded

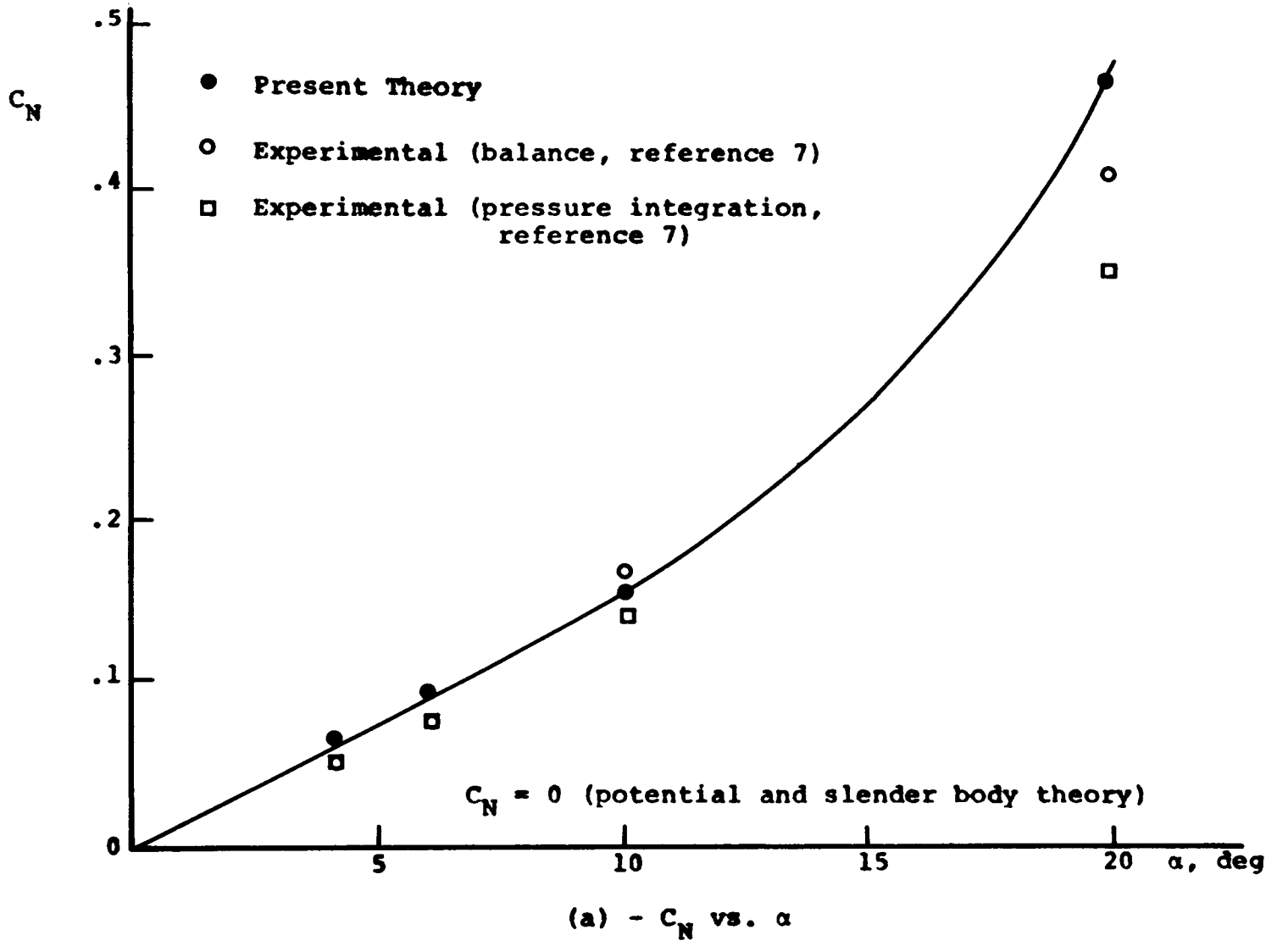

(a) - C_N vs. α

Figure 14 - Aerodynamic Characteristics of Ellipsoid.

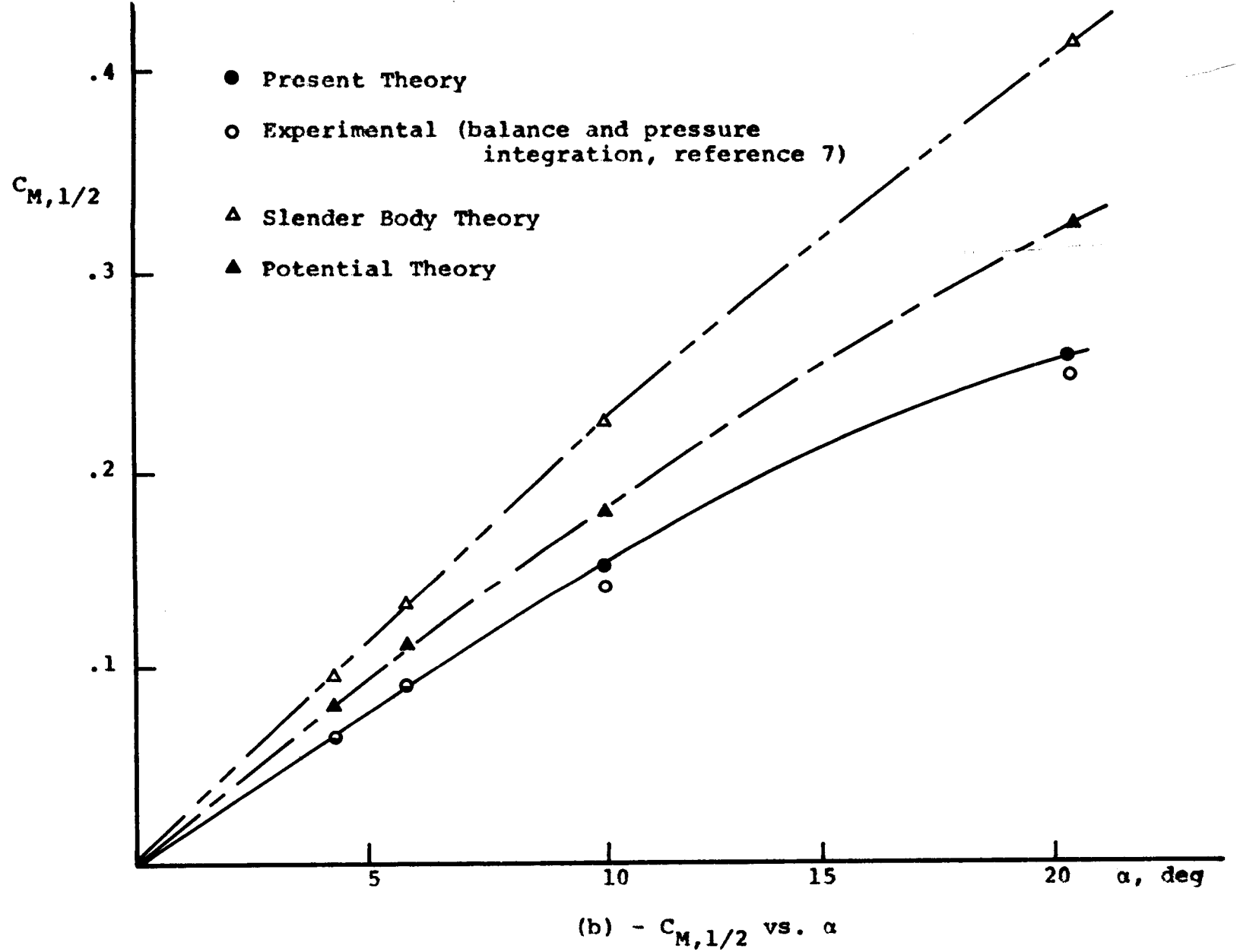

(b) - $C_{M,1/2}$ vs. α

Figure 14 - Concluded

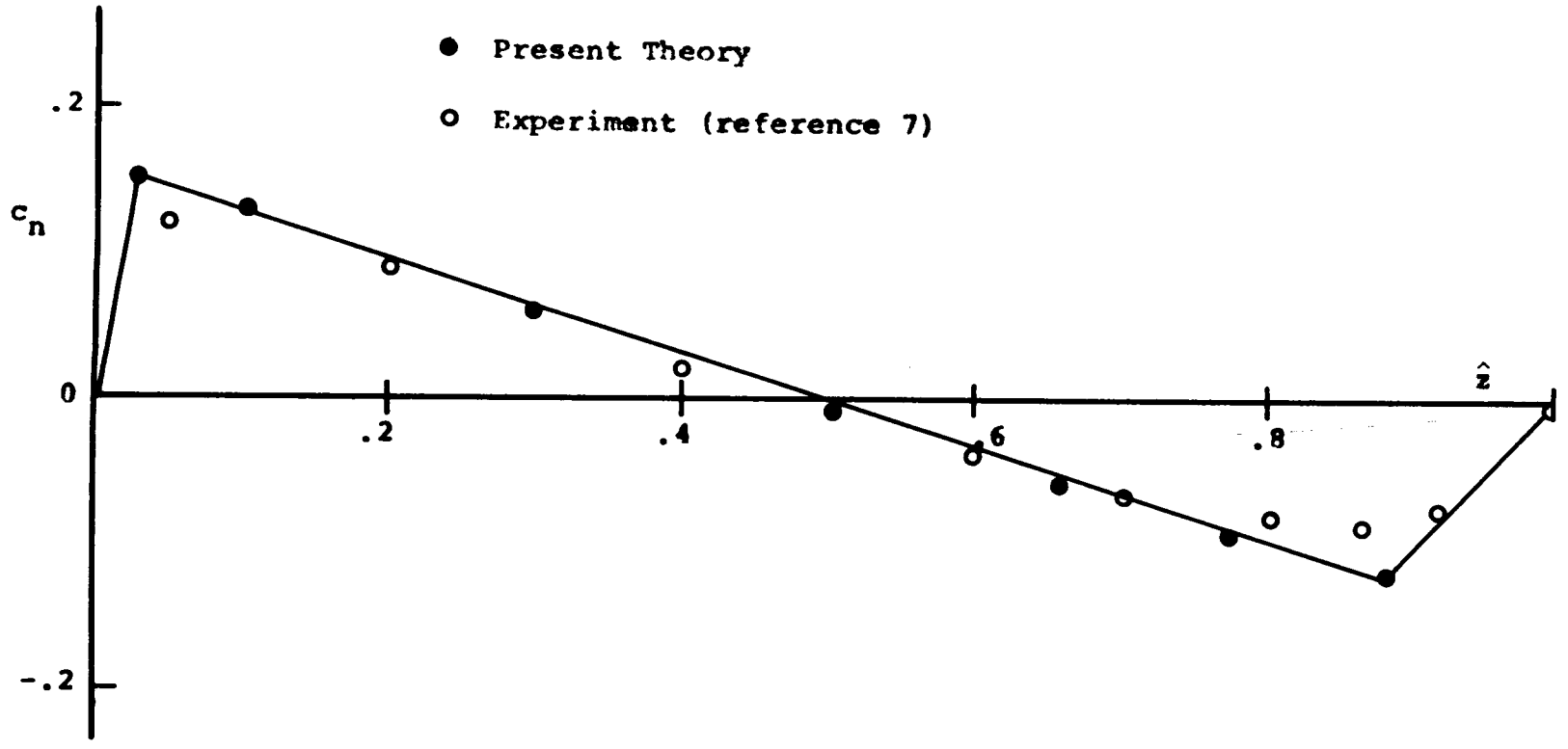

(a) - $\alpha = 6°$

Figure 15 - Normal Force Distribution Over Ellipsoid.

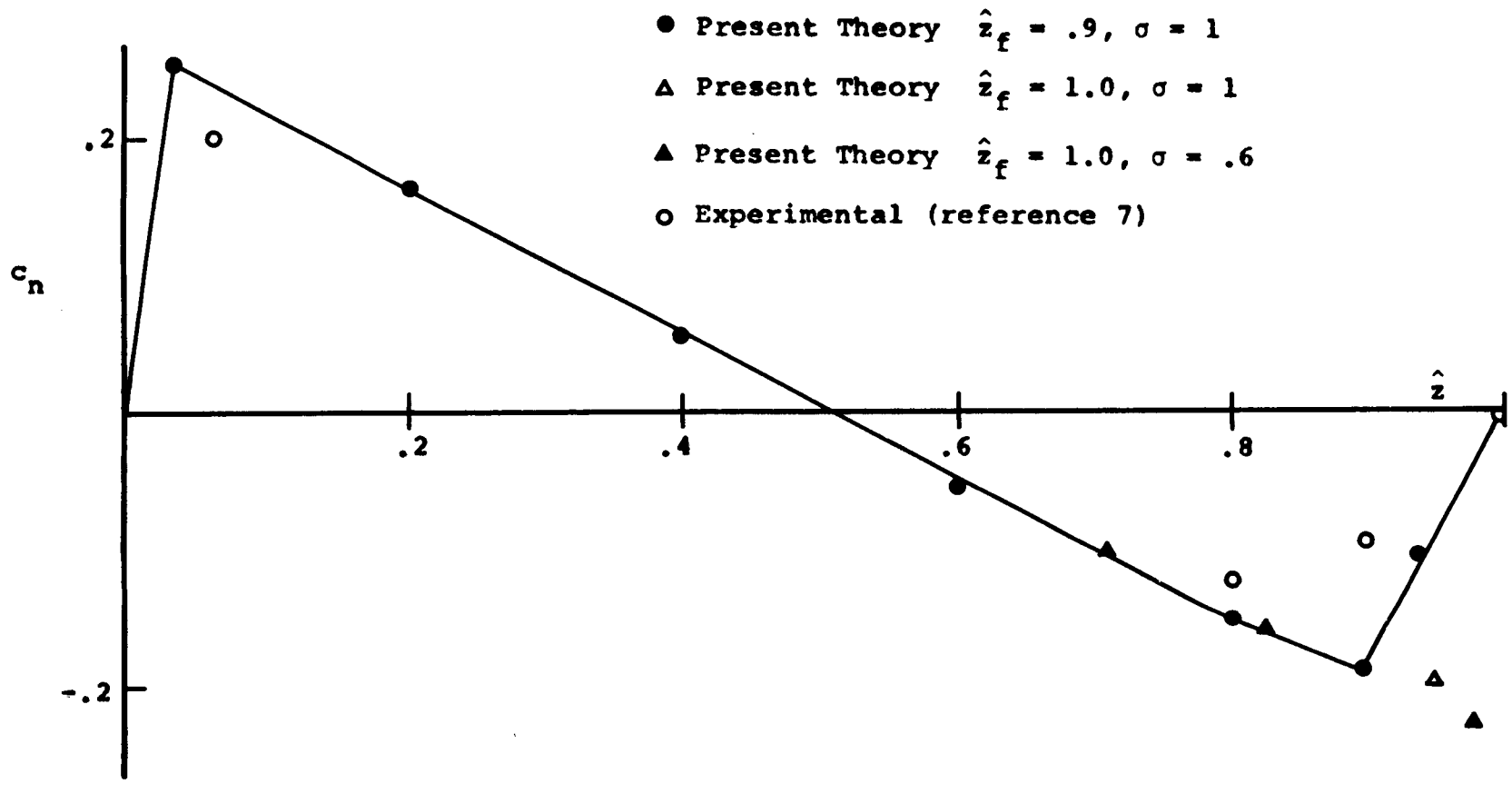

(b) - α = 10°

Figure 15 - Continued

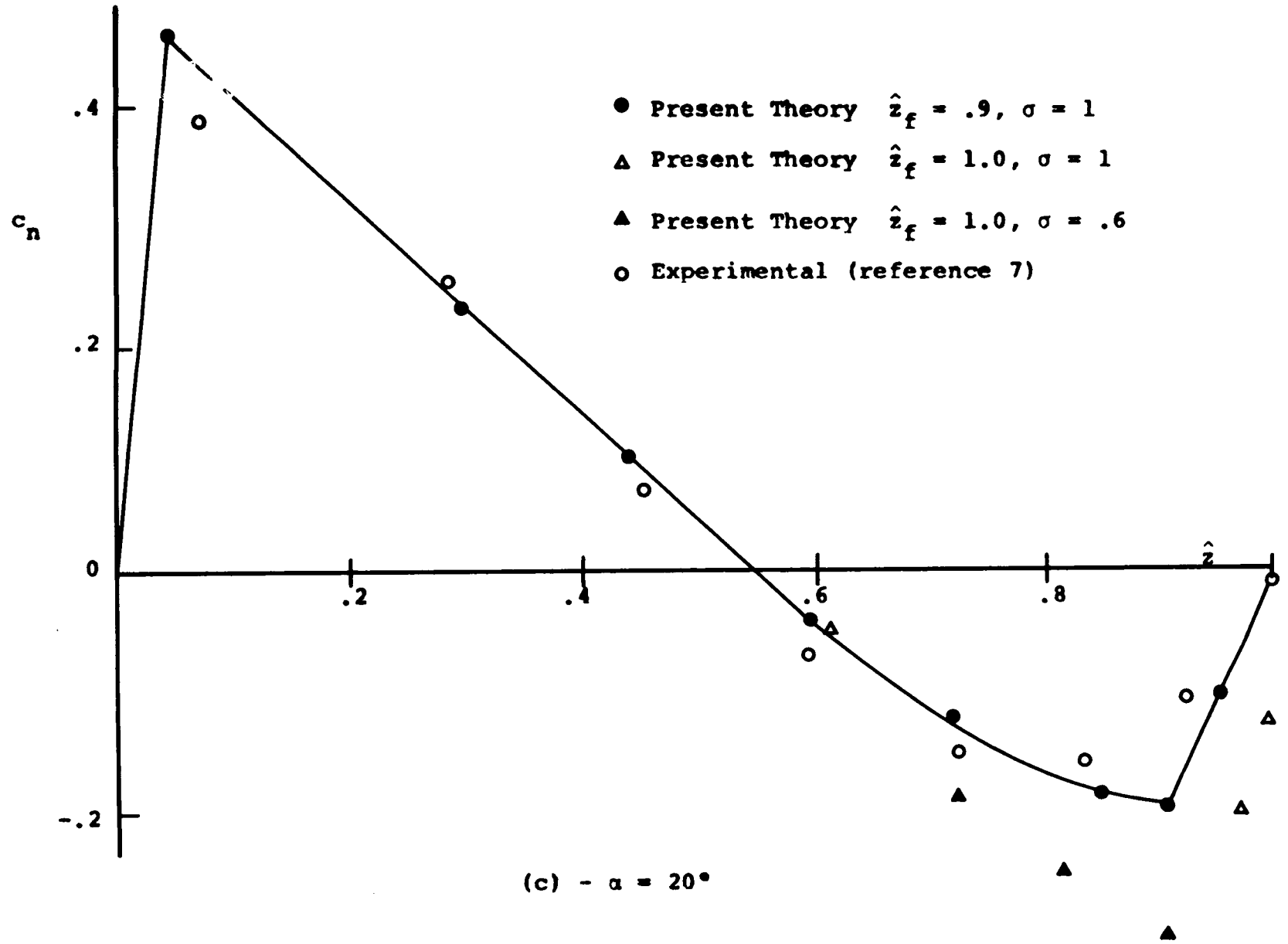

(c) - α = 20°

Figure 15 - Concluded

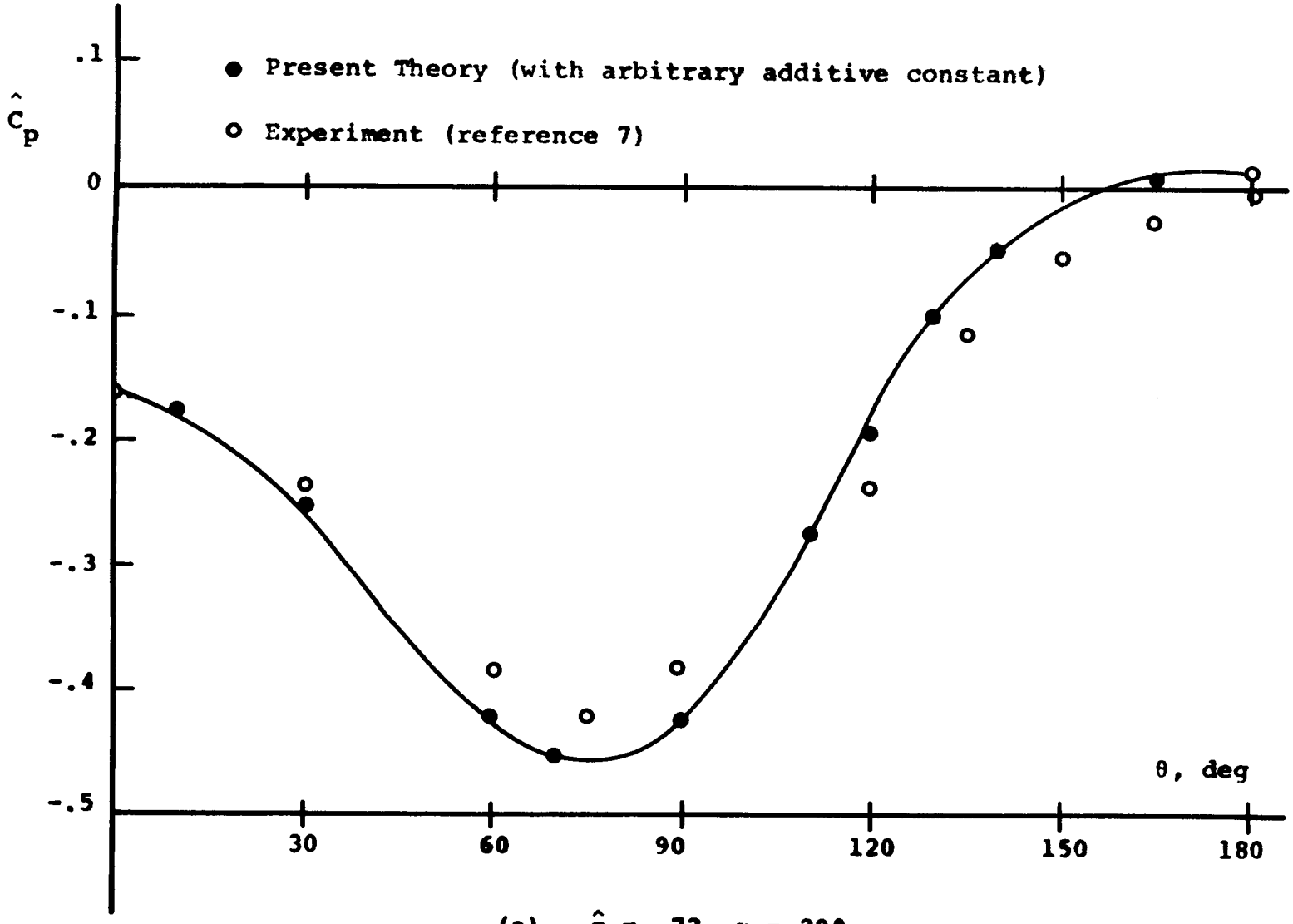

(a) - $\hat{z}$ = .72, α = 20°

Figure 16 - Pressure Distribution on Ellipsoid.

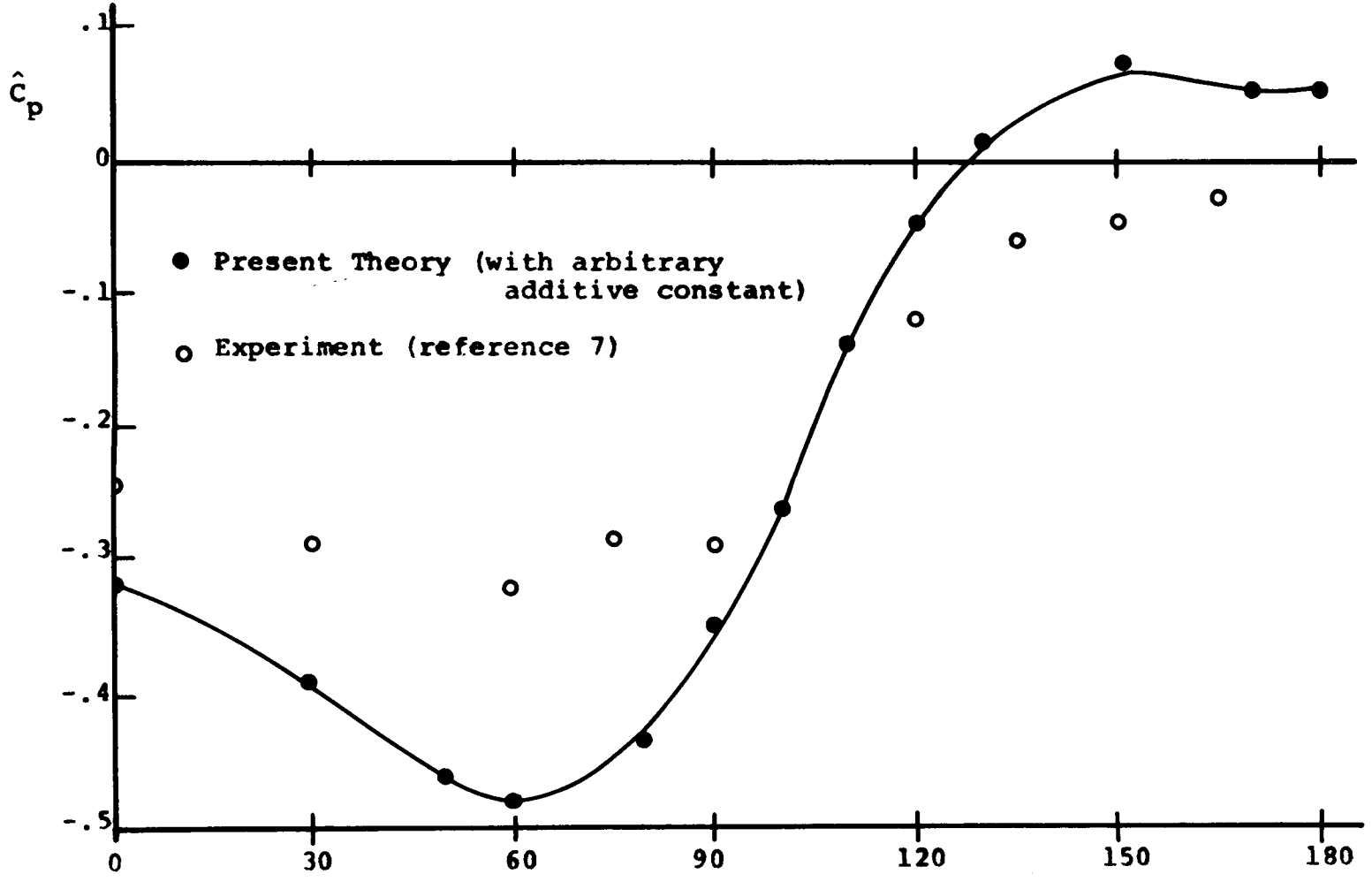

(b) - $\hat{z}$ = .863, α = 20°

Figure 16 - Continued

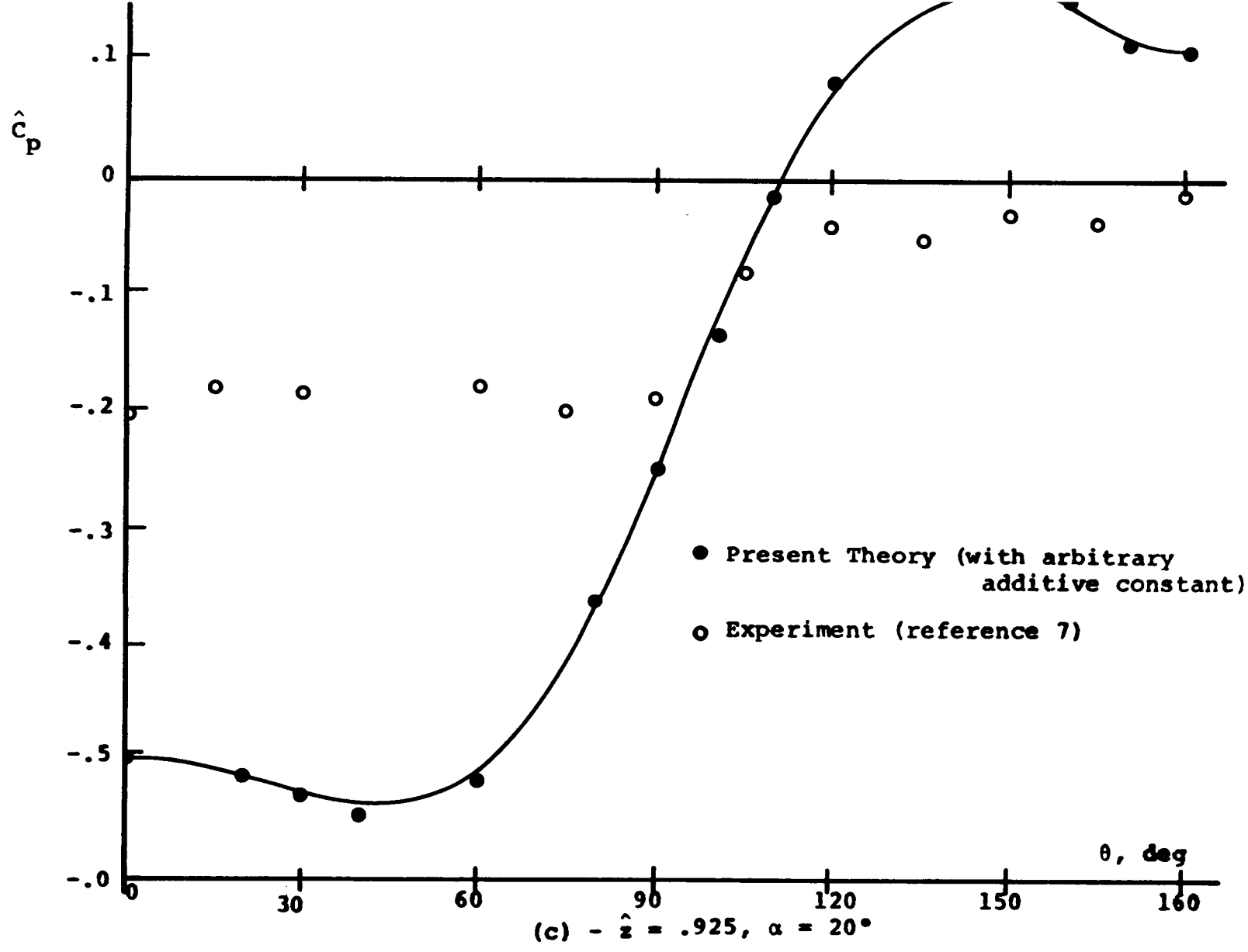

(c) - $\hat{z}$ = .925, α = 20°

Figure 16 - Concluded

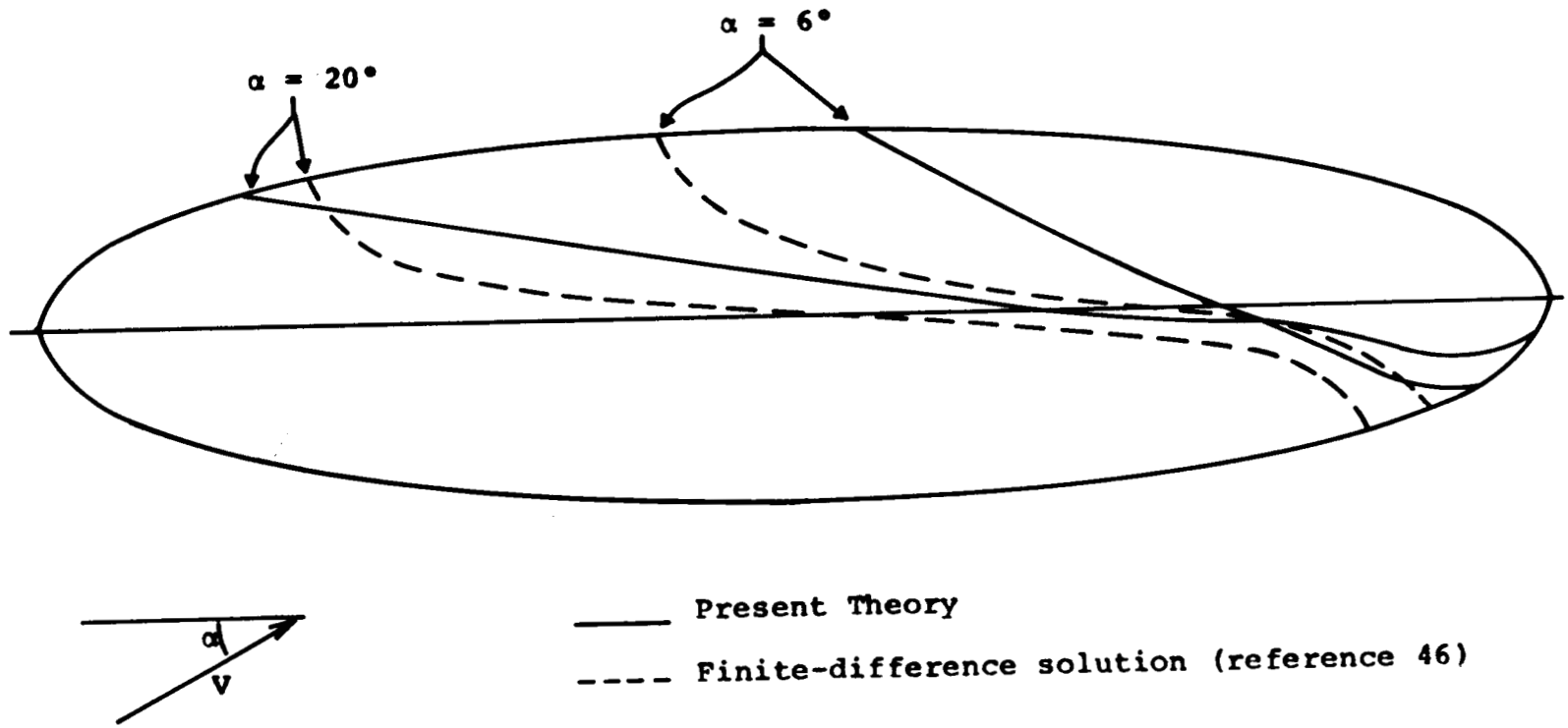

Figure 17 - Theoretical Separation Regions on Ellipsoid.

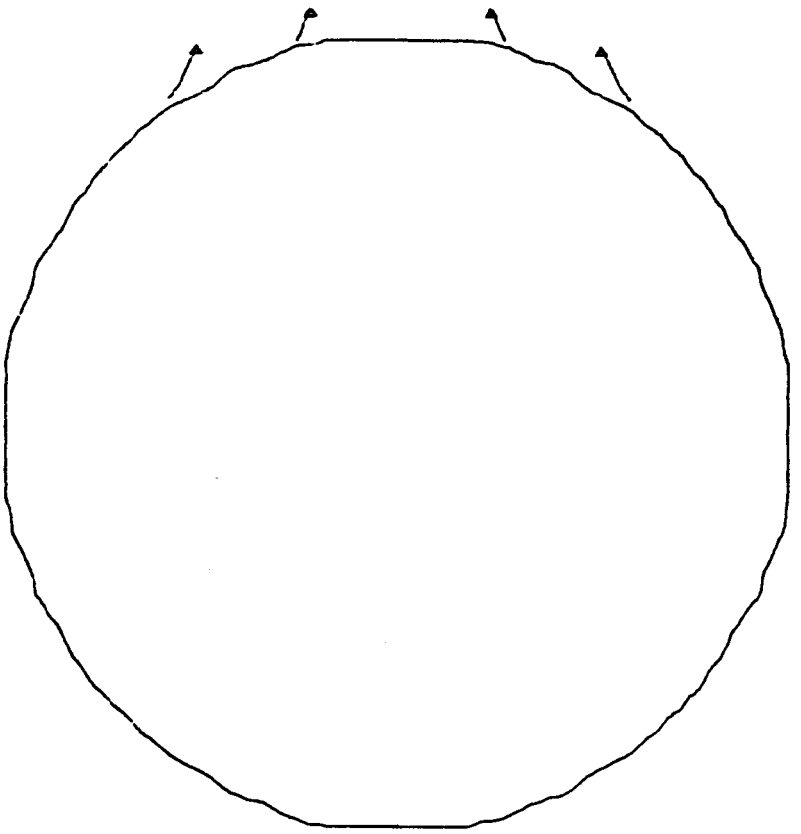

(a) - $\hat{z} = .197$, $\alpha = 20°$

Figure 18 - Wake Pattern of Ellipsoid.

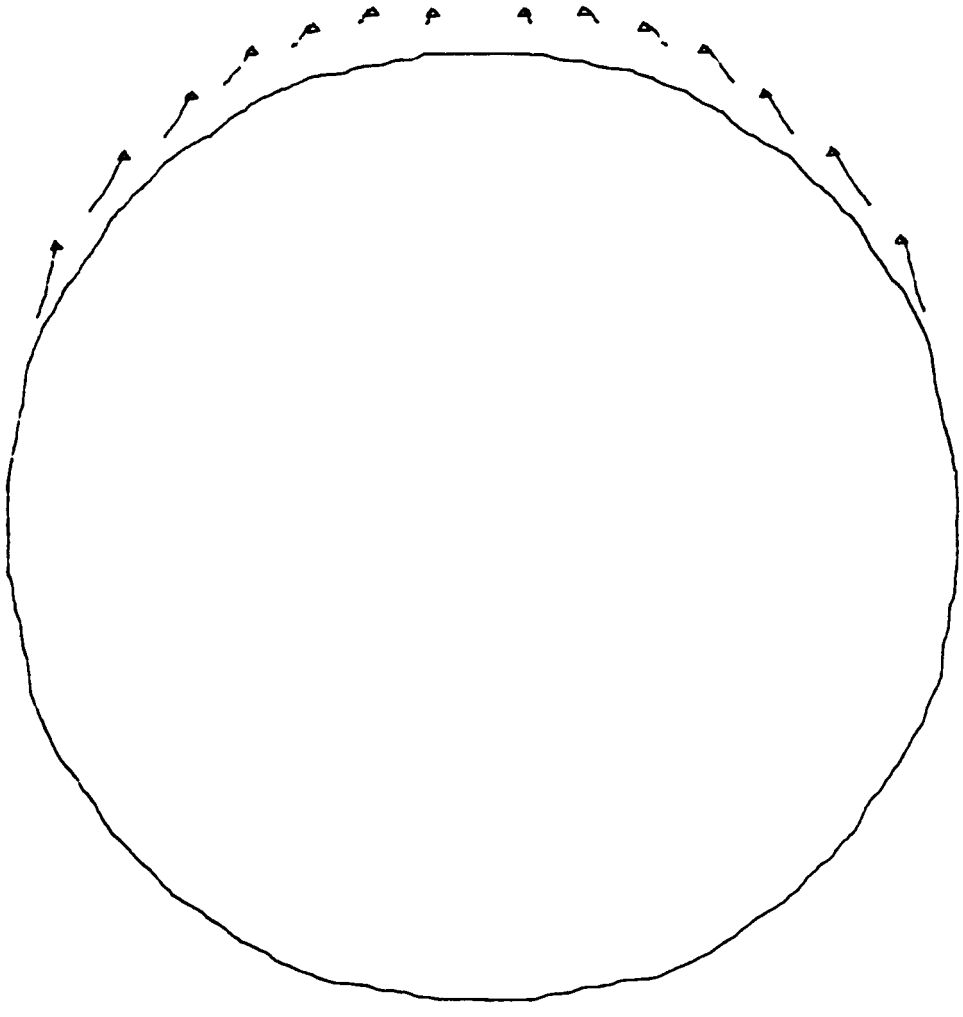

(b) - $\hat{z} = .363$, $\alpha = 20°$

Figure 18 - Continued

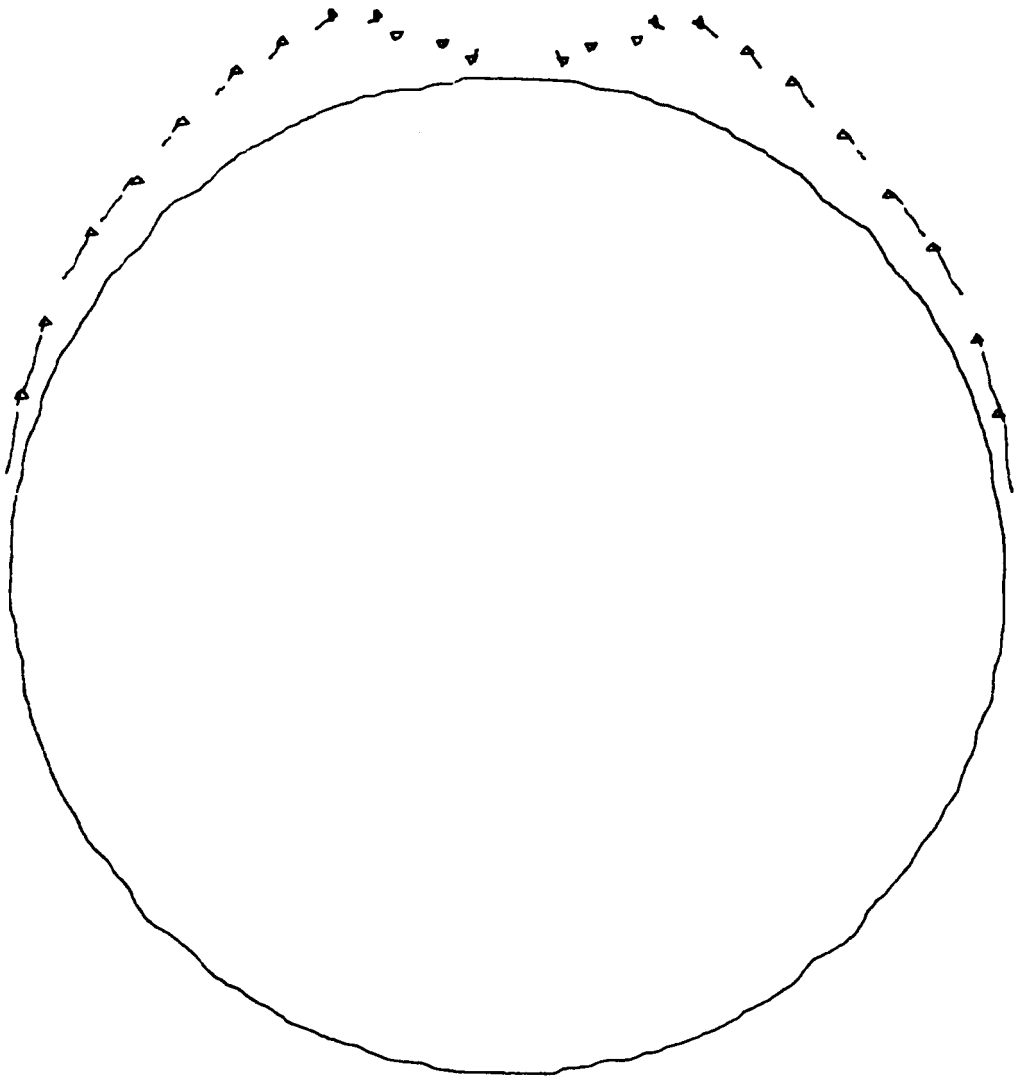

(c) - $\hat{z} = .530$, $\alpha = 20°$

Figure 18 - Continued

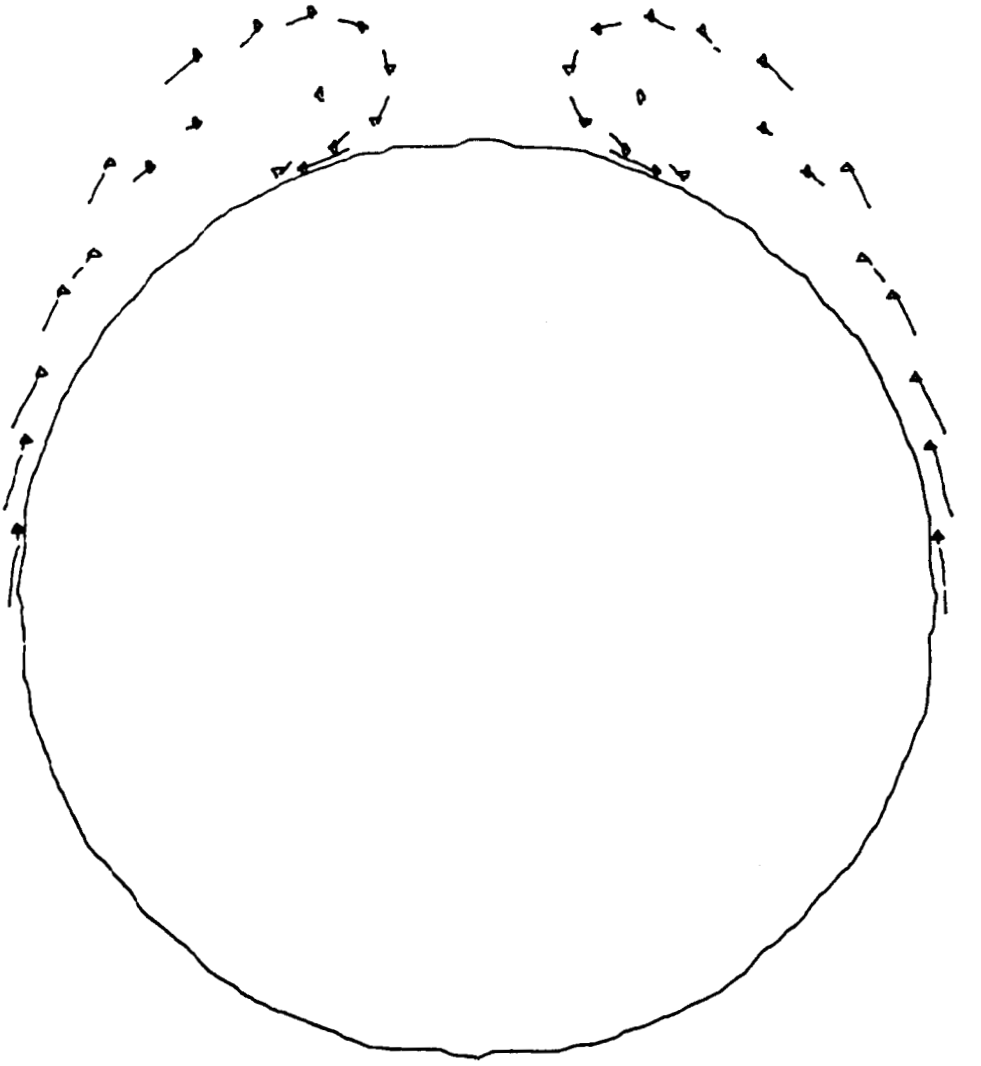

(d) - $\hat{z}$ = .700, α = 20°

Figure 18 - Continued

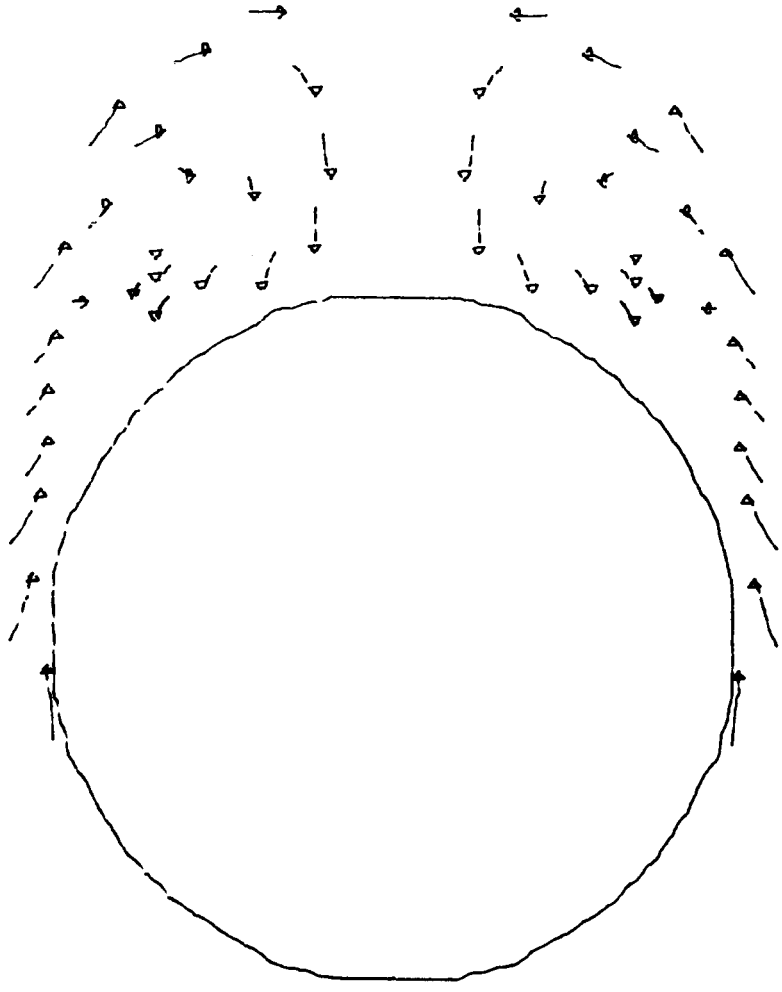

(e) - $\hat{z} = .863$, $\alpha = 20°$

Figure 18 - Concluded